HHS Public Access

Author manuscript

Nat Immunol. Author manuscript; available in PMC 2022 April 06.

Published in final edited form as:

Nat Immunol. 2021 September ; 22(9): 1118–1126. doi:10.1038/s41590-021-00984-4.

Human autoinflammatory disease reveals ELF4 as a transcriptional regulator of inflammation

Paul M. Tyler[1,‡], **Molly L. Bucklin**[1,‡], **Mengting Zhao**[1,‡], **Timothy J. Maher**[1], **Andrew J. Rice**[1], **Weizhen Ji**[2,3], **Neil Warner**[4], **Jie Pan**[4], **Raffaella Morotti**[5], **Paul McCarthy**[3], **Anne Griffiths**[4], **Annemarie M.C. van Rossum**[6], **Iris H.I.M. Hollink**[7], **Virgil A.S.H. Dalm**[8], **Jason Catanzaro**[3], **Saquib A. Lakhani**[2,3], **Aleixo M. Muise**[4], **Carrie L. Lucas**[1,2,*]

[1]Immunobiology Department, Yale University School of Medicine, New Haven, CT, USA

[2]Pediatric Genomics Discovery Program, Yale University School of Medicine, New Haven, CT, USA

[3]Department of Pediatrics, Yale University School of Medicine, New Haven, CT, USA

[4]SickKids Inflammatory Bowel Disease Center and Cell Biology Program; Research Institute, Hospital for Sick Children; Department of Pediatrics and Biochemistry, University of Toronto, Hospital for Sick Children, Toronto, ON, Canada

[5]Department of Pathology, Yale University School of Medicine, New Haven, CT, USA

[6]Department of Pediatrics, Division of Pediatric Infectious Diseases and Immunology, Erasmus University Medical Center, Rotterdam, the Netherlands

[7]Department of Clinical Genetics, Erasmus University Medical Center, Rotterdam, the Netherlands

[8]Department of Internal Medicine, Division of Clinical Immunology and Department of Immunology, Erasmus University Medical Center, Rotterdam, the Netherlands

Abstract

Transcription factors specialized to limit the destructive potential of inflammatory immune cells remain ill-defined. We discovered loss-of-function variants in the X-linked ETS transcription factor gene *ELF4* in multiple unrelated male patients with early-onset mucosal autoinflammation and inflammatory bowel disease (IBD) characteristics including fevers and ulcers that responded to IL-1, TNF or IL-12p40 blockade. Using cells from patients and newly generated mouse

*Correspondence: Carrie.Lucas@yale.edu.

‡These authors contributed equally

Author contributions: *P.M.T., M.L.B.,* and *M.Z.* performed experiments, analyzed data, and wrote the manuscript. *T.J.M.,* and *A.J.R.* performed experiments and analyzed data. *W.J.* performed analysis of genomics data from family A. *N.W.* identified and evaluated the *ELF4* variant in patient B.1. *J.P.* performed staining of biopsy samples from patient B.1 and analyzed data. *R.M.* provided pathology expertise for staining of biopsy samples from patient A.1. *P.M.* provided clinical care and insights for patient A.1. *A.G.* provided clinical care and insights for patient B.1. *A.M.C.vR.* provided clinical care and insights for patient C.1. *I.H.I.M.H.* performed genetic analysis of family C. *V.A.S.H.D.* recruited and provided clinical care and insights for patient C.1. *J.C.* recruited and provided clinical care and insights for patient A.1. *S.A.L.* oversaw genetic analysis of family A. *A.M.M.* provided clinical care and oversaw genomics analysis and histology staining of biopsies from of family B. *C.L.L.* supervised overall research and data analysis, performed experiments, and wrote/edited the manuscript. All authors discussed and reviewed the manuscript.

Competing interests: S.A.L. is part owner of Qiyas Higher Health and Victory Genomics, startup companies unrelated to this work. All other authors declare no competing interests.

models, we uncovered that ELF4-mutant macrophages had hyperinflammatory responses to a range of innate stimuli. In mouse macrophages, Elf4 both sustained the expression of anti-inflammatory genes such as *Il1rn* and limited the upregulation of inflammation amplifiers, including *S100A8*, *Lcn2*, *Trem1* and neutrophil chemoattractants. Blockade of Trem1 reversed inflammation and intestine pathology in mice carrying the same mutations in Elf4 challenged with lipopolysaccharide *in vivo*. Thus, ELF4 restrains inflammation and protects against mucosal disease, a discovery with broad translational relevance for human inflammatory diseases such as IBD.

Discovery of causative single-gene mutations in severe immune diseases of childhood provides a powerful and unbiased lens through which physiologically relevant immune regulatory mechanisms can be elucidated directly from humans. Collectively, these disorders affect millions of patients with an estimated prevalence of 1 in every 5000 people, and greater than 400 distinct monogenic inborn errors of immunity have been described to date.[1,2] However, many such disorders remain undiscovered and undiagnosed. Unbiased next-generation genomic DNA sequencing of patients and their parents, paired with stringent filtering approaches[3–6], enables powerful new insights into the genetic basis of rare human disease while also triggering new and broadly applicable basic science questions. Here, we report the discovery of a monogenic human disorder caused by pathogenic variants in *ELF4*, an X-linked ETS transcription factor gene, in multiple male patients who presented with mucosal inflammation in childhood.

The ETS family of transcription factors consists of 29 members in humans and 28 members in mice, with a well-conserved ETS DNA-binding domain that recognizes a core consensus sequence defined *in vitro* as 5-'GGAA' [7,8]. Differing expression patterns, upstream activators and binding partners endow different ETS proteins with non-redundant functions. ELF4 was originally called 'myeloid Elf1-like factor' (MEF), and a variety of functions have been attributed to Elf4 in mouse studies[9]. Notably, Elf4 regulates NK cell development and perforin expression[10], $CD8^+$ T cell proliferation[11], anti-viral immunity through type I IFN[12], constitutive expression of housekeeping genes in macrophages[13], and T_H17 cell differentiation.[14] Elf4 knockout (KO) mice develop normally but are more susceptible to West Nile Virus[12] infection and experimental autoimmune encephalomyelitis.[14]

We describe a human autoinflammatory disease we term 'deficiency in ELF4, X-linked' (DEX) in three male patients with fever, oral ulcers and mucosal inflammation. Using primary patient cells and newly generated mouse models, either lacking Elf4 or expressing the patient-derived missense Elf4 variant, we discovered neutrophilic infiltration associated with elevated expression of IL-17 and increased pro-inflammatory responses of macrophage as mechanisms underlying the inflammation in DEX patients. Elf4 KO macrophages failed to sustain the transcription of key anti-inflammatory genes and instead upregulated proinflammatory genes, including *Trem1*, a transmembrane receptor with potent amplifying effects on inflammation[15], within hours of stimulation. The hyperresponsiveness of Elf4 KO macrophages was observed with numerous pattern recognition receptor (PRR) stimuli and could be reversed *in vitro* and *in vivo* by blockade of Trem1.

Results

Patients with mucosal autoinflammation harbor ELF4 variants

The proband, patient A.1, is a European-American male who was healthy for the first two years of life before he began experiencing fevers of unknown origin associated with abdominal pain and diarrhea for 2–3-day intervals over a one-year period. An abdominal ultrasound revealed pan-colitis with diffuse wall thickening (8 mm) and hypervascularity of the entire colon. Colonoscopy revealed scattered aphthous-like ulcerations throughout the colon, and oral ulcers (canker sores) were also noted. HLA-B51, associated with Behcet's disease, was negative, and genetic testing for the 7 commonest periodic fever syndromes (e.g., Familial Mediterranean Fever) was also negative. Given the duration of symptoms (approximately one year), the cause of acute colitis was not thought to be infectious, and immunohistochemistry was negative for adenovirus, cytomegalovirus and fungi (Supplementary Table 1). Instead, the patient's age, imaging and pathology findings were more consistent with an inflammatory bowel disease (IBD)-like disorder with possible monogenic cause[16]. Suboptimal immunoglobulin response to the live, attenuated measles-mumps-rubella vaccine was noted. Flow cytometry of peripheral blood mononuclear cells (PBMCs) showed intermittently low NK cells and low CD27+ memory B cells, but was otherwise normal (Supplementary Table 1, Extended Data Fig. 1a–g). Treatment with steroids or IL-1 blockade ameliorated symptoms.

Patient B.1 is a European-Canadian male who presented at 9 years of age. He has a history of fevers, persistent perianal ulcers and fissures, oral ulcers and mild anemia without a documented family history of IBD. Upper endoscopy revealed evidence of chronic gastritis, esophagitis and some eosinophils (3/hpf). Lower endoscopy demonstrated a healing perianal abscess without induration, marked lymphonodular hyperplasia of the cecum, including ileocecal valve, and a single ulcerated lesion in the terminal ileum. Histology showed acute inflammation in the terminal ileum suggestive of ulceration and chronic inflammation with lymphonodular hyperplasia of the ileocecal valve. Persistence of the lesions prompted an immune workup, which revealed lymphocytosis, thrombocytosis and elevated ESR with normal IgG and IgE, normal T cells and slightly elevated B cells. Suboptimal immunoglobulin response to the live, attenuated measles-mumps-rubella vaccine was noted. Evaluation was thought to be consistent with atypical Behcet's disease, and the patient responded to IL-12p40 blockade.

Through GeneMatcher[17], we identified a European-Dutch male (patient C.1) who presented at 13 years of age with a papulopustular skin reaction with ulcerations on the inner thighs. Shortly thereafter, he experienced severe balanitis, and treatment involved acute circumcision, which was complicated by granulomatous reactions. Bacterial cultures were negative and antibiotics ineffective. Subsequently, antifungal treatment was initiated and the skin lesions gradually improved. A few weeks later, he suffered from a severe *C. albicans* oral fungal infection, resulting in loss of weight due to reduced intake from severe mouth pain requiring an additional course of antifungal agents. He then suffered from recurrent *C. albicans*-positive aphthous lesions of the mouth and throat, requiring multiple courses of antifungals. Since the age of 18 years, his clinical picture has been dominated by culture-

negative oral ulcers and aphthous lesions that respond to steroid treatment (prednisone) and TNF blockade (Supplementary Table 1).

Whole exome sequencing (WES) on genomic DNA from the three families identified two distinct and pathogenic variants in the X-linked transcription factor *ELF4* (NM_001421) (Fig. 1a, Supplementary Table 2). The proband patient A.1 has a *de novo* missense variant (NC_000023.10:g.129205072C>G using GRCh37) that results in substitution of tryptophan to serine at codon 251 (c.752G>C, p.W251S). Patient B.1 has a maternally inherited hemizygous *ELF4* nucleotide change identical to that as seen in patient A.1. Finally, patient C.1, born from consanguineous parents, has a maternally inherited frameshift variant (NC_000023.10:g.129203447delC using GRCh37) that results in a premature stop codon (c.1015delG, p.A339fs*32). Sanger sequencing confirmed the WES findings (Fig. 1b). Neither variant is present in the gnomAD database of >210,000 human exomes or genomes [18], and algorithms predicting deleteriousness assess both as pathogenic with a CADD score >25 for p.W251S [5,19]. Alignment of the human ELF4 DNA-binding ETS domain with ETS domains from genes in other species, including *D. melanogaster* and *C. elegans*, highlights W251 as a completely conserved amino acid (Fig. 1c) that forms a hydrogen bond with the backbone of DNA (Fig. 1d). The W251S ELF4 variant is rarer and has a higher CADD score than variants with a MAF cutoff of $>10^{-4}$ in males in gnomAD (Fig. 1e). Moreover, missense variants are depleted from the nucleotides of *ELF4* encoding the conserved ETS DNA-binding domain (Extended Data Fig. 1k), underscoring predicted deleteriousness of the W251S variant in the ETS domain. As predicted, patient PBMCs contain detectable mRNA and protein for the W251S variant but loss of both mRNA and full-length protein for the A339fs variant (Fig. 1f–g). We also observed loss of ELF4 protein in lysates from THP1 cells after CRISPR targeting of *ELF4* (Extended Data Fig. 1j), confirming the antibody specificity for ELF4. We next co-transfected 293 cells with vectors expressing the myc-tagged ELF4 wild-type (WT), W251S or 339Afs variant and a luciferase reporter to measure ELF4 transcriptional activity and found both mutants exhibited loss of transcriptional activity (Fig. 1h) but all of the ELF4 variants from gnomAD with a MAF cutoff of $>10^{-4}$ had normal transcriptional activity (Fig. 1h and Extended Data Fig. 1l). Thus, we defined a cohort of patients with a previously uncharacterized monogenic human disorder we termed ‘deficiency in ELF4, X-linked’ (DEX).

To further investigate and model the effects of ELF4 deficiency, we generated *Elf4*-deficient C57BL/6 mice, which lack Elf4 protein (hereafter Elf4 KO, Extended Data Fig. 1m–n). We also generated point-mutant C57BL/6 mice harboring the W250S missense variant equivalent to the human W251S (hereafter W250S mice, Extended Data Fig. 1m and 1o). We assessed *ELF4* allele usage in PBMCs from the heterozygous mother of patient B.1 and in both $CD4^+$ and $CD8^+$ T cells from heterozygous female W250S mice and saw the missense allele comprised >50% of cDNA clones (Extended Data Fig. 1p–q), indicating no apparent fitness cost to hematopoietic cells of the W251S/W250S ELF4 variant. ELF4 was reported to promote perforin expression[10]. $CD8^+$ T cells from Elf4 KO or W251S mice (Extended Data Fig. 1r), DEX patients (Extended Data Fig. 1s) or $CD8^+$ T cells from healthy human that were CRISPR/Cas9-edited to induce the deletion of ELF4 (Extended Data Fig. 1t–u) had reduced perforin expression when expanded and activated with IL-2 to induce the differentiation of cytotoxic T lymphocytes (CTL) compared to wild-

type littermate, healthy donor or non-targeted CRISPR/Cas9 controls. Moreover, perforin expression in CTL from patients A.1, B.1, and C.1 was increased by overexpressing myc-tagged WT, but not W251S ELF4 (Extended Data Fig. 1v). As such, T cell phenotypes in DEX patients, healthy human T cells with CRISPR deletion of *ELF4* and both Elf4 KO and W250S mice indicate that the patient-derived *ELF4* variants are loss-of-function.

Inflamed mucosal tissue in DEX patients is infiltrated by neutrophils

Histological analysis of colon (Fig. 2a) and cheek (Fig. 2b) biopsies from DEX patients demonstrated pathological changes associated with neutrophilic infiltration of the inflamed mucosa (Fig. 2a–b). Flow cytometry on PBMCs from patient A.1 indicated borderline low numbers of NK cells, $CD27^+$ memory B cells and a trend toward increased numbers of naïve ($CD45RA^+CCR7^+$) $CD4^+$ and $CD8^+$ T cells compared to healthy control subjects (Extended Data Fig. 1a–g). NK cell killing (Extended Data Fig. 1h) and production of IFN-α2 after lipopolysaccharide (LPS) stimulation of PBMCs were normal compared to healthy control subjects (Extended Data Fig. 1i). [20–23] Serum CXCL1 was significantly elevated in DEX patients A.1 and C.1 over healthy donor controls (Fig. 2c). Calprotectin, a biomarker correlated with the severity of intestinal inflammation, was elevated in stool samples from patient A.1 (Fig. 2d), while most serum analytes measured were within the range of healthy controls (Extended Data Fig. 2a). Treatment with anakinra, and subsequently with canakinumab to block IL-1, normalized the neutrophilia and CRP readouts in patient A.1 (Fig. 2e–f). In a 2% DSS-induced colitis model [24,25], Elf4 KO and W250S mice exhibited more severe colon pathology (Fig. 2g–h), increased spleen cellularity (Fig. 2i) and an increase in activated $CD4^+$ T cells and $CD11b^+Ly6G^+$ myeloid cells in the colon relative to wild-type littermate controls (Fig. 2j–k). Together, these data indicate a key role for ELF4 in regulation of inflammation, which is conserved between humans and mice.

ELF4 deficiency augments inflammatory T_H17 cell responses

Partly due to their role in recruiting neutrophils, IL-17-producing T_H17 cells are known to contribute to IBD, and ELF4 has been reported to suppress T_H17-mediated inflammation in mice [14]. Using immunofluorescence microscopy, we detected elevated expression of IL-17A and RORγT in ascending colon biopsies from DEX and IBD patients compared to healthy control (Fig. 3a–c). Purified naïve $CD4^+CD25^-CD127^+CD45RO^-$ T cells from DEX patient A.1 differentiated *in vitro* with IL-1β and IL-23 (T_H17 conditions) for 7 days (Extended Data Fig. 3a)[21] produced more IL-17A compared to healthy control (Fig. 3d). In addition, $CD4^+$ T cells from Elf4 KO or W250S mice showed enhanced production of IL-17A when differentiated with either IL-1β, IL-23 and IL-6 (pro-inflammatory conditions) or TGF-β and IL-6 (less inflammatory conditions) compared to wild-type littermate controls (Fig. 3e and Extended Data Fig. 3b,c). There was no significant difference in the percentage of naïve $CD4^+$ T cells in DEX patients or Elf4 KO or W250S mice compared to wild-type controls (Extended Data Fig. 3d–e). When injected intraperitoneally with the stimulatory CD3 antibody 2C11, which induces myeloid cell-dependent inflammatory T cell responses[26], Elf4 KO and W250S mice exhibited a significantly higher frequency of IL-17A-producing $CD4^+$ T cells upon restimulation of splenocytes compared to wild-type littermate controls (Fig. 3f), indicating W250S behaved similarly with the Elf4 KO mice. Moreover, ELF4 was constitutively nuclear in $CD4^+$ T effector cells (Extended Data Fig. 3f), and there was no

activation difference between WT and Elf4 KO $CD4^+$ T cells as measured by upregulation of CD69 and CD25 after *in vitro* stimulation with antibodies for CD3 and CD28 (Extended Data Fig. 3g).

RNA sequencing indicated an enrichment in the expression of inflammatory-response genes (GO:0006954) in naïve Elf4 KO $CD4^+$ T cells at baseline (i.e., prior to any stimulation) compared to wild-type littermate controls, based on gene set enrichment analysis (GSEA) and KEGG pathway analysis (Fig. 3g and Extended Data Fig. 3h–k). T_H17-related genes (*Il17a*, *Il17f*, *Ccr6*, and *Il1r1*) and inflammatory GO terms were induced in W250S $CD4^+$ T cells 48 hours after T_H17 differentiation in vitro (Fig. 3h–i). ATAC-seq identified 832 peaks specifically enriched in Elf4 KO naive $CD4^+$ T cells, a majority of which was upregulated compared to wild-type littermates (Extended Data Fig. 3l–m). Based on both ATAC-seq and RNA-seq, a subset of these genes, representing genes involved in chromatin regulation, was significantly differentially regulated in Elf4 KO and W250S CD4 T cells compared to wild-type CD4 T cells (Extended Data Fig. 3n). Thus, ELF4 restrained the differentiation of T_H17 cells, which are known to promote mucosal inflammation and neutrophil recruitment, in human and mouse.

ELF4 broadly suppresses macrophage responses

Next, we investigated the role of ELF4 in monocytes and macrophages, which highly expressed ELF4 (Extended Data Fig. 3o). We evaluated a broad panel of inflammatory cytokines in the culture supernatants of PBMCs from patients A.1 and B.1 and ten healthy donor controls following stimulation with lipopolysaccharide (LPS), a TLR4 stimulus relevant at mucosal barriers. Of the cytokines evaluated, the pyrogens IL-1β and IL-6 were elevated in the supernatants from patient cells (Fig. 4a and Extended Data Fig. 4a), and intracellular IL-12p40 was elevated in patient monocytes (Fig. 4b). Elevated production of IL-1β and CXCL1 was also detected in monocyte-derived macrophages from healthy donors in which ELF4 was deleted using CRISPR before stimulation with LPS (Fig. 4c and Extended Data Fig. 4c). LPS-stimulated monocytes from patients A.1 and B.1 showed normal production of IL-10 and responsiveness to IL-10 (Extended Data Fig. 4a–b), a key anti-inflammatory gene known to regulate mucosal and intestinal inflammation. In order to determine whether and to what extent deletion of ELF4 caused a hyperinflammatory phenotype in macrophages, we used bone marrow-derived macrophages (BMDMs) from Elf4 KO and W250S mice. IL-1β, IL-6, IL-12p70, IL-23 and CXCL1 were increased after LPS stimulation in BMDMs from W250S mice compared to wild-type littermates (Fig. 4d). Stimulation with additional PRR ligands, including muramyl dipeptide (MDP, a NOD2 agonist), polyI:C (a TLR3 agonist) and β-glucan (a dectin-1 agonist), which represent relevant innate stimuli at sites of mucosal inflammation induced increased IL-1β, IL-6, IL-23 and CXCL1 production in Elf4 KO and W250S BMDMs compared to wild-type littermate controls (Fig. 4e–f and Extended Data Fig. 4d).

We next assessed the innate immune cell-mediated inflammation and endotoxic shock in response to intraperitoneal administration of LPS. Elf4 KO and W250S mice displayed a more severe drop in body temperature (Fig. 4g) and increased clinical score (Extended Data Fig. 4e) compared to wild-type littermate controls following the administration of 2 mg/kg

LPS. IL-1β, IL-6, IL-23 and CXCL1 were elevated and IFN-β was reduced in the serum of Elf4 KO and W250S mice compared to wild-type littermate controls 4 hours after challenge (Fig. 4h, Extended Data Fig. 4f, and Supplementary Table 3), along with higher expression of IL-18 and IL-33 at 24 hours post-LPS challenge (Fig. 4i). Female mice heterozygous for the W250S *Elf4* allele exhibited no change in response to i.p. LPS compared to wild-type female littermates (Extended Data Fig. 4g–h), suggesting that one wild-type allele can prevent excessive inflammation in mice. Collectively, these data demonstrate that ELF4 is a broad and potent regulator of inflammatory macrophage responses.

ELF4 promotes IL1RN and limits Trem1 expression in macrophages

To further define the molecular drivers of the broad inflammatory phenotype in the Elf4-deficient macrophages, we performed RNA-seq in BMDMs from Elf4 KO and wild-type mice at baseline and 4 or 16 hours after stimulation with LPS. As expected, the most downregulated gene was *Elf4*, while most differentially expressed genes (DEGs) mapped to immune and inflammatory pathways (Extended Data Fig. 5a–f). At 16 hours post-LPS stimulation, Elf4 KO BMDMs had significantly lower expression of a set of genes with anti-inflammatory functions, including *Tnfsf10* (encoding TRAIL), *Il10*, *Il18bp*, *Il1rn*, *Batf2*, *Cd274* (encoding PD-L1), *Il27* and *Trex1*, compared to wild-type BMDMs (Fig. 5a and Extended Data Fig. 5m). Reduced expression of *Il10* and *Il1rn* was also detected at 16 hours post-LPS stimulation in BMDMs derived from W250S mice compared to wild-type littermates (Extended Data Fig. 5g–h). The clinical efficacy of anakinra, a therapeutic version of the protein encoded by *IL1RN*, in patient A.1 (Fig. 2e–f) prompted us to examine *Il1rn* further. Analysis of previously published chromatin immunoprecipitation (ChIP) data in mouse BMDMs[13] indicated the presence of a putative binding peak for Elf4 in *Il1rn* as well as *Batf2*, *Cd274*, *Il27* and *Trex1* (Fig. 5a). RT-PCR indicated the normal initial induction of *Il1rn* mRNA in Elf4 KO BMDMs at 4 hours post-LPS treatment and an increasingly significant reduction in *Il1rn* transcripts at the 8-, 16- and 24-hour post-LPS compared to wild-type BMDMs from littermate controls (Fig. 5b). When overexpressed in 293T cells, WT, but W251S ELF4, induced significant activation of a luciferase reporter containing the region of genomic DNA upstream of the transcription start site (TSS) of *IL1RN*, which contained conserved ETS-binding sites (Fig. 5c and Extended Data Fig. 5i).

Because the hyperinflammatory responses in Elf4 KO macrophages were detected as early as 4 hours post-LPS challenge, we next investigated the transcriptional responses at this timepoint. A set of pro-inflammatory genes, which included *S100A8* (encoding a calprotectin subunit), *Trem1*, *Il36g* (formerly called *Il1f9*), *Il19*, *Ptges*, *Mefv*, *Cxcl3*, *Lcn2* (lipocalin-2) and *Cxcl2* (Fig. 5d) were significantly upregulated at 4 hours post-LPS stimulation in Elf4 KO BMDMs compared to BMDMs from wild-type littermates, and previously published ChIP-seq datasets demonstrated Elf4 binding upstream of a subset of these genes (Fig. 5d and Extended Data Fig. 5j)[13]. Expression of *S100a8* and *Trem1* was also increased in BMDMs derived from Elf4 KO and W250S mice at 4 hours post-LPS stimulation (Extended Data Fig. 5k–l). Trem1 is a surface protein with roles in amplifying inflammation [15]. Trem1 mRNA and protein were upregulated in Elf4 KO compared to wild-type BMDMs 4 hours after stimulation with LPS, as indicated by RT-PCR and flow cytometry (Fig. 5e–f). The LPS-induced production of pro-inflammatory cytokines in Elf4

KO BMDMs, including IL-1β, CXCL1, IL-6, IL-12 and IL-23, was reversed by the addition of a Trem1-Fc fusion protein, which blocks the interaction of Trem1 with its ligands (Fig. 5g and Extended Data Fig. 5n–p). Moreover, i.p. administration of Trem1-Fc one hour after the i.p. LPS challenge in the Elf4 KO mice rescued the body temperature drop and the score for severity of clinical symptoms (Fig. 5h and Extended Data Fig. 5q) and reversed the increase of inflammatory cytokines in the serum (Fig. 5i and Extended Data Fig. 5r) and small intestine pathology (Fig. 5j) [27]. As such, myeloid-derived pyrogens and cytokine inducers of IL-17 were elevated in humans and mice lacking functional ELF4, and this was consistent with the fever and mucosal inflammation documented in the DEX patients. Our results indicate that the hyperinflammatory responses in Elf4-deficient myeloid cells were due to loss of expression of anti-inflammatory genes, such as *IL1RN*, and a Trem1-dependent amplification of inflammation.

Discussion

Monogenic autoinflammatory diseases offer the potential to discover genes and pathways regulating inflammation in humans[28]. We report here that the ETS transcription factor ELF4 is a negative regulator of inflammatory disease. Patients lacking functional ELF4 exhibit heightened mucosal inflammation with fever and ulcers throughout the GI tract, especially in the mouth. This pathology, similar to Behcet's or orofacial Crohn's disease, is associated with elevated expression of innate cytokines. Based on our data in three unrelated patients and their mouse models, we define this disorder as 'deficiency in ELF4, X-linked' (DEX).

In contrast to several other ETS factors, loss of ELF4 does not result in large defects in immune cell lineages. Prior mouse studies had not hinted the role of ELF4 as a broad regulator of inflammatory responses, and we suspect that this is partly because spontaneous clinical disease is not observed in Elf4-deficient mice due to housing in specific pathogen-free laboratory conditions [29,30]. Upon challenge with DSS, however, we detected augmented inflammatory responses in the colon of Elf4 KO and W250S mice compared to wild-type littermate controls. Our analyses focused on contributions of ELF4 to regulation of inflammatory T cells and macrophages, and future investigations are necessary to dissect cell type-specific functions of ELF4 in immune and epithelial cells [31].

Defective type I IFN responses have been reported in Elf4 KO mice [12]. Elf4 is induced by type I interferon and feeds forward to increase interferon production and hundreds of interferon-stimulated genes (ISGs)[12,32]. We confirmed low IFN-β in the serum of LPS-challenged Elf4 KO and W250S mice compared to wild-type littermate control mice and in *Ifnb1* reporter assays containing multiple interferon-stimulated response elements (ISREs). There is currently no evidence for increased susceptibility to common viral infections in the three DEX patients studied here, and we found no evidence for a viral cause of the ulcers. However, it remains unknown whether DEX patients would fail to mount sufficient anti-viral responses to rarer and more pathogenic viruses. ELF1, the closest paralog of ELF4, has been implicated in the regulation of a subset of non-canonical ISGs [33], raising the possibility that ELF4 could have a similar nuanced role in the regulation of ISRE-driven ISGs. Beyond anti-viral control, type I IFNs are known to have anti-inflammatory functions, particularly through the negative regulation of IL-1 and IL-18 and of inflammatory T_H17 cells [34–36].

The specific contribution of dysregulated type I IFN responses to hyperinflammatory macrophages and T_H17 cells in DEX remains to be determined.

Elf4 was reported to act as a transcriptional activator bound to cis-regulatory elements upstream of housekeeping genes in BMDMs, though the effect of Elf4 deficiency on gene expression was not reported[13]. Following LPS stimulation in BMDMs, we detected time-dependent changes in expression in anti-inflammatory genes such as *IL1RN,* which required ELF4 for sustained expression. *IL1RN* encodes the endogenous IL-1 receptor antagonist, a potent negative regulator of the IL-1 response. IL-1 is a pyrogen that drives the production of IL-17 from lymphocytes to further amplify inflammation and neutrophil recruitment. The therapeutic efficacy of anakinra, a recombinant version of the IL-1 receptor antagonist, in patient A.1 supports the key contribution of IL-1 in DEX pathology. Although *IL1RN* expression is affected in DEX, its early induction is normal and, therefore, systemic inflammation in DEX is less severe than in patients with loss-of-function variants in *IL1RN* [37,38]. Additionally, effective treatment with blockers of IL-12p40, a shared subunit of IL-23 and IL-12, or with blockers of TNF in patients B.1 or C.1, respectively, underscores the contributions of IL-1 and IL-23 as inducers of IL-17 and TNF in disease etiology.

LPS stimulation in Elf4 KO macrophages upregulated hundreds of genes, including *S100a8* (encoding a calprotectin subunit), *Trem1*, *Lcn2* (lipocalin-2), *Cxcl2* and *Cxcl3*, among others. Excessive production of these inflammatory genes in Elf4 KO mice relative to wild-type controls point to an anti-inflammatory role for ELF4 in TLR signaling. I.p. LPS challenge revealed significantly greater changes in body temperature, inflammatory serum proteins and small intestine pathology in Elf4 KO and W250S mice compared to wild-type littermates. These effects were reversed by blockade of Trem1, an amplifier of innate immunity and inflammation [15,39]. Because exposure of tissue macrophages to PRR ligands from commensals and other microbes is most pronounced at the gastrointestinal mucosa, the lack of functional ELF4 to regulate the local inflammatory tone causes these tissues to be most affected in DEX patients. Taken together, the characterization of a monogenic mucosal autoinflammatory disease in humans with an ELF4 deficiency and the mechanistic studies in human and mouse define ELF4 as a central transcriptional regulator of inflammation.

Methods (see Supplementary Table 4 for resource information)

Human subjects research

All human subjects in this study provided informed consent to use their samples for research and to publish de-identified genetic sequencing data, in accordance with Helsinki principles for enrollment in research protocols that were approved by the Institutional Review Boards of Yale University, Hospital for Sick Children, and Erasmus University Medical Center. Blood from healthy donors was also obtained under approved protocols. All relevant ethical regulations for work with human participants were followed.

Animal research and generation of CRISPR-engineered Elf4 mouse strains

Mouse studies received ethical approval from Yale University's Institutional Animal Care and Use Committee (IACUC) and were in compliance with all relevant ethical

regulations for animal testing and research. For newly generated mouse strains, Cas9 mRNA and sgRNA were injected into fertilized mouse oocytes. Elf4 KO mice were generated with crRNA sequences: GCAGAGGGAGAGGTAGTGAA and AAGATCTTAGTGATCCCTTG. Point mutant knock-in mice were generated with sgRNA sequence: CAAGGCTGTGTCCAAGCTGT. Embryos were implanted into mice and founder animals were generated with breeding to WT female C57BL/6 mice. Heterozygous females born were used to back-cross ten generations.

Whole-exome and Sanger sequencing

Genomic DNA was prepared from peripheral blood using standard procedures. The whole exome was captured using xGen target kit from IDT, and 99 base paired end sequencing on the Illumina platform (HiSeq 4000) was performed under a research protocol at the Yale Center for Genome Analysis. The sequence reads were converted to FASTQ format and were aligned to the reference human genome (hg19). GATK best practices were applied to identify genetic variants, and variants were annotated by ANNOVAR [41,42]. The trio samples were sequenced to a mean depth of 51–60X independent reads per targeted base, with at least 20 independent reads in 91% of targeted bases. WES data for Patient B.1 and his mother (duo) was obtained using a NimbleGen VCRome capture kit and sequenced on an Illumina HiSeq 2500 platform as previously described [43].

Quantitative RT-PCR

Cells were resuspended in RLT lysis buffer (added 10uL/mL beta-mercaptoethanol) and spun down in a Qiashredder at the highest speed for 4 minutes. RNA was isolated using the Qiagen RNeasy Plus Mini Kit following the standard protocol. Synthesis of cDNA from at least 200 ng RNA was performed with Reverse Transcriptase Superscript III and poly (dT) for priming according to manufacturer's instructions. For RT-PCR, cDNA was diluted 1:5 in water and 2.5 ul was used per well as template with Sybr Green supermix. Primers used are included in Supplementary Table S5.

SDS-PAGE and immunoblotting

Cells for western blotting were lysed with 1x RIPA buffer, supplemented with protease inhibitors and phosphatase inhibitors. Clarified lysates were boiled with sample buffer in SDS for 5 minutes at 95°C and loaded into pre-cast 12 well polyacrylamide stain-free gels. Anti-ELF4 was purchased from Proteintech, and detects an ELF4 band at ~100 kDa (Extended Data Fig. 1j). Secondary antibodies were from SouthernBiotech. Uncropped immunoblots are shown in Supplementary Fig. 1.

Cell lines and CRISPR

THP1 cells (human monocyte cell line) were purchased from ATCC and cultured in RPMI supplemented with 100 U/ml penstrep, glutamine, and 10% fetal bovine serum. CRISPR RNPs were prepared by annealing crisprRNA, tracrRNA, and Cas9 and transfected into cells with Lonza buffer SG. ELF4 gRNAs were used individually or in combination to generate KO cell lines, see Supplemental Table S5 for sequences.

Luciferase reporter assays

Myc-tagged ELF4 overexpression constructs (500 ng) were co-transfected with promoter luciferase reporters (50 ng) using turbofectamine into 293T cells into each well of a 24 well plate when cells reached >60% confluency, and supernatants were harvested for analysis with luciferase substrate 24 hours later. Luminescence values were recorded with a Tecan plate reader. The previously described ELF4 activity reporter using mouse *Ifnb1* promoter and multiple ISRE sites for Fig. 1h was purchased. *ELF4* variants from the gnomAD database used in functional assays were those present in males at a minor allele frequency $>10^{-4}$ in order to compare activity of these higher-prevalence variants against the reference allele and the patient-derived variants. A plasmid with each of the patient variants and most of the rare variants from the healthy population were created by mutagenesis cloning with a primer pair containing the desired variant in the middle of the primers. For the rare variants with high GC content at the desired site, short gblock fragments containing the desired variants were ordered (IDT) and subsequently amplified and cloned into the rest of the *ELF4* gene. Reporter vector with secreted luciferase gene was purchased. Endogenous regulatory sequences (~350 base pairs upstream of predicted TSS) were subcloned into the luciferase reporter vector using restriction enzymes BamHI and SpeI. Mutagenesis cloning for three separate ETS sites in the regulatory sequences of IL1RN was performed by PCR with Phusion polymerase mix. Each core GGAA element was substituted with an AAAA to abolish ETS binding.

Analysis of allele usage in heterozygous females

PBMCs were isolated from peripheral blood of B.1 and his parents by ficoll gradient centrifugation. RNA extraction and cDNA synthesize done as described. PCR amplification around the W251S variant were used to clone this region in a vector, followed by bacterial transformation of the product. Individual colonies were selected for colony PCR using primers that anneal to the vector, and amplicons were purified with a Qiagen Min-Elute PCR cleanup kit. PCR products were sanger sequenced and frequencies of colonies containing W251 or S251 were determined in order to estimate the allele frequency of the reference and missense variants. Splenocytes from a heterozygous W250S mouse were sorted into pure populations of $CD4^+$ or $CD8^+$ cells using an Aria, and allele frequencies estimated as described above.

Serum protein measurements

Patient and healthy donor serum was collected. Human serum concentrations of cytokines and chemokines were measured using the 42-Plex Human Cytokine/Chemokine Assay and 65-Plex Human Cytokine/Chemokine Assay (Eve Technologies).

NK cell cytotoxicity assay

The ability of NK cells to kill targets was assessed using a 4-hr Cr^{51} release assay assessing percent lysis of labeled K562 cell targets after incubation with PBMCs at various effector-to-target ratios.

Flow cytometry analysis

Flow cytometry data was analyzed by FlowJo 10.5. Quantification graphs for ELISAs, flow cytometry cell populations, etc. were generated using Prism GraphPad. Gating strategies are demonstrated in Supplementary Fig. 1.

DSS-induced experimental colitis

Colitis was induced by the addition of 2% (w/v) 36,000–50,000MW DSS to drinking water for 7 days. Colitis severity was monitored daily through changes in body weight and stool consistency. At experimental endpoints, colon and spleen were harvested and processed for flow cytometric analysis/histology. Colons were dissociated from fat, and luminal contents were gently removed. Tissues were opened longitudinally, cut into 1-cm pieces and washed by vortexing in ice-cold PBS. Tissue pieces were subsequently incubated with a stripping solution (10 mL HBSS, 4mM EDTA, 1mM 1,4-Dithiothreitol at 37C with vigorous shaking for 20 min to remove epithelial cells. Enzymatic digestion was performed in DMEM medium containing 1 mg/mL Type II Collagenase, 0.5 mg/ml Dispase II and 50 u/ml DNAse II type V. Tissue suspensions were mechanically dissociated and passed through a 70 μm cell strainer. Intestinal single-cell suspensions were then harvested at the interface of a 40/80% (v/v) Percoll gradient and washed thoroughly in ice-cold PBS containing 2% (v/v) FBS before proceeding to further analysis. Spleen suspensions were mechanically dissociated through a 70 μm filter and subjected to ACK lysing buffer prior to washing twice in ice-cold PBS for analysis. A total histological severity score, ranging from 0 to 6, was obtained by summing inflammatory cell infiltrate (mucosa:1, mucosa and submucosa:2, transmural:3) and intestinal architecture (focal erosions:1, erosions±focal ulcerations:2, extended ulcerations±granulation tissue ±pseudopolyps:3).

In vivo anti-CD3 challenge and analysis of splenic T cell responses

WT and Elf4 KO mice were injected intraperitoneally at hours 0, 48, and 96 with 20 μg of anti-CD3 antibody in 200 μL of PBS or PBS-only control. Mice were sacrificed at day 5 of anti-CD3 challenge, and the spleen and mesenteric lymph nodes were separated and mashed over a 70-micron filter in a suspension of complete RPMI 1640. Cells were washed with PBS, red blood cells lysed with ACK, washed with media, and resuspended/counted. Approximately 10 million cells from mesenteric lymph nodes and 25 million splenocytes from each mouse were activated with 1 μg/mL PMA, 1 μg/mL Ionomycin, and 5 μg/mL Brefeldin A in complete RPMI 1640. After incubation for 6 h, cells werencubated for 15 min on ice (dark) in 200 μL PBS with fixable viability dye eFluor 450, then stained with anti-CD4 Pacific Blue and anti-I-A/I-E APC/Cy7 for 45 minutes on ice. Cells were centrifugated and washed with FACS buffer in between each step. Cells were fixed and stained with eBioscience Foxp3/Transcription Factor Staining Buffer Set according to the manufacturer's instructions and stained with antibodies: anti-IFNγ PE/Cy7 or Rat IgG_1, κ isotype Ctrl PE/Cy7, anti-IL-17A Alexa Fluor 647 or Rat IgG_1, κ isotype Ctrl Alexa Fluor 647.

Immunohistochemistry, antibodies and confocal microscopy

Sigmoid biopsy specimens collected from normal, IBD without ELF4 deficiency and the patients for this investigation were obtained before the drug treatment or without other clinical therapy. Rabbit polyclonal antibodies were obtained against ELF4, FOXP3, RORγT, IL10, IL17 and mouse monoclonal cytokeratin.

Dual Immunofluorescent Histochemical Staining: The details of IF staining on FFPE sections are published [44]. Briefly, as a first step, paraffin was removed using Xylene, and afterwards rehydrated with different percentages of ethanol. Antigen retrieval was performed with high-pressure cooking in EDTA–borax buffer (1mM EDTA, 10mM borax, 10mM boric acid with 0.001% Proclin 300 at pH 8.5. To block non-specific staining, the slides were incubated for 1 hr at room temperature in 4% BSA in 1 X phosphate-buffered saline 20% normal donkey serum. A proper diluted primary antibody, polyclonal antibody and anti-IL10 or RORγ T mouse monoclonal antibody incubation was performed overnight at 4°C. On the following day, stained slides were washed three times for 5 min with 3 × PBS. Secondary antibody, donkey anti-rabbit IgG Fab2 fragment-Rhodamine conjugate mixed with donkey anti-mouse IgG Fab2 fragment-FITC conjugate incubation was performed at room temperature in darkness for 2 hrs, and slides were washed afterwards three times for 10 min in darkness. As a nuclear counterstain reagent, RedDot2 far red fluorescence was used at a dilution of 1:200. Finally, sections were mounted overnight with Vector shield fluorescence mounting medium (Vector Labs).

Confocal microscopy: Double/triple-immunostained sections were obtained using a Leica confocal laser scanning microscope (model TCS-SP8) and LAS-AF software (Leica Microsystems, Wetzlar, Germany). The variable excitation wavelengths of the krypton/argon laser were 488 nm for fluorescein isothiocyanate conjugate, 568 nm for Texas Red complex, and 695 nm for Alexa Fluor 680 conjugate/RedDot 2 (nuclear counterstaining). Image processing, including color resolution, color separation, and merging of fields, was carried out using Adobe Photoshop CS5 software.

T_H17 cultures

PBMCs were isolated from healthy donor buffy coats or patient blood using Ficoll separation. Naïve CD4 T cells were further purified using the EasySep Naïve CD4+ T Cell Isolation Kit II or sorted using fluorescence activated cell sorting (stained for live/dead (eBioscience Fixable Viability Dye eFluor 780), CD4 PE/Cy7, CD25 PE, CD45RO, and CD127 BV650. Cells were plated a concentration of 0.05–0.15E6 cells/mL in 200 μL cRPMI (RPMI supplemented with 10% FBS and 1% penicillin, streptomycin, and glutamine) with viability of 90% or greater. 96-well U-bottom plates were coated for at least 2 hours at 37°C with 50 μL per well at 5 μg/mL anti-CD3 in PBS. The original 50 μL of PBS was removed and washed with 150 μL of PBS before plating cells. Master mixes for each condition consisted of anti-CD28 (2 μg/mL) anti-IFNy (2 μg/mL), anti-IL-4 (2 μg/mL), IL-1β (25 ng/mL), and IL-23 (25 ng/mL) as described. Cells were resuspended and plated in the given master mix, then incubated at 37°C for 6–7 days before supernatants were collected to be analyzed for IL-17A by ELISA.

For mouse T_H17 cultures, cells were harvested from WT and Elf4 KO mouse spleens and lymph nodes, filtered through a 70-micron filter using FACS buffer (PBS + 2% FBS), spun down at 350xg for 5 minutes, lysed in Ack lysis buffer to remove red blood cells, and resuspended in MACS buffer (PBS, 2 mM EDTA, 0.5% BSA) for total CD4+ T cell isolation. CD4+ T cells were then obtained using the Miltenyi total CD4+ Isolation Kitand subsequently stained with anti-CD4 Pacific blue, anti-CD25 PE, anti-CD62L APC, and anti-CD44 FITC to obtain CD4+CD25-CD44-CD62L+ naïve CD4+ T cells via cell sorting on a BD FACS Aria machine. Cells were counted resuspended in media, then plated at a concentration of 0.1E6 cells/mL in 200 μL cRPMI (RPMI supplemented with 55 μM beta mercaptoethanol, 10% FBS and 1% penicillin, streptomycin, and glutamine) with a viability of 90% or greater. 96-well U-bottom plates were coated for at least 2 hr at 37°C with 50 μL per well 10 μg/mL anti-CD3 in PBS. The original 50 μL of PBS was removed and washed with 150 μL of PBS before plating cells. Master mixes for each condition consisted of anti-CD28 (1.5 μg/mL), anti-IFNγ (2 μg/mL), anti-IL4 (2 μg/mL), IL-1β (25 ng/mL), IL-23 (20 ng/mL), IL-6 (20 ng/mL), and TGFβ (5 ng/mL) as described. Cells were resuspended and plated in the given master mix, then incubated at 37°C for 3–4 days before supernatants were collected to be analyzed via ELISA and cells harvested for re-stimulation and subsequent staining/flow cytometry analysis.

Cytoplasmic and nuclear fractionation

1–10 × 10^6 T effector cells were lysed and extraction of separate cytoplasmic and nuclear protein fractions was performed using the NE-PER Kit according to the manufacturer's instructions. The same was performed for activated Tregs and Teffectors at day 6. 4x sample buffer completed with 5% beta-mercaptoethanol was added, and lysates were boiled at 95°C. Approximately 10–20 ug of total protein was separated using stain-free SDS-PAGE gels and transferred to a nitrocellulose membrane. Images of total protein loading using Bio-Rad stain-free imaging were obtained, and membranes were blocked with 5% nonfat dry milk in Tris-buffered saline (TBS) with 0.01% Tween-20 (TBST) for 1 hr at room temperature before incubating with primary antibody overnight at 4°C. After washing with TBST for 1 hr at room temperature, HRP-conjugated secondary antibody was added for an additional hour at room temperature. After a 1-hr wash step, HRP substrate was added to the membranes, which were then subjected to chemiluminescent imaging using the ChemiDoc Touch Imaging System.

RNA sequencing and gene set enrichment analysis (GSEA)

Cells were resuspended in RLT lysis buffer (added 10uL/mL beta-mercaptoethanol) and spun down in a Qiashredder at the highest speed for 4 minutes. RNA was isolated using the Qiagen RNeasy Plus Mini Kit following the standard protocol. Quality of RNA was assessed using a Nanodrop Spectrophotometer. Samples were then stored at −80°C until submitted for RNA-sequencing differential gene expression analysis at the Yale Center for Genomic Analysis. 500–1000ng of RNA was submitted for each sample. Sequencing conditions included whole exome capture, NovaSeq instrument, HiSeq paired-end 100bp sequencing read length, and 25,000,000 reads/sample. Analysis of RNA-sequencing data was performed using Partek software, in which Bowtie 2 was using to establish aligned reads and genes were filtered using FDR = 0.05, fold change ≥ 2.

Generated datasets were normalized using TMM normalization and downloaded from Partek. GSEA 4.0.3 was used and standard protocol was followed. Datasets were uploaded as a .txt file, phenotype labels generated in Texmaker and uploaded as .cls file, and gene sets were downloaded from the GSEA official website uploaded as a .gmt file. The inflammatory response gene set (GO: 0006954) was from the C5 collection of GO gene sets under biological processes. Run parameters include: number of permutations 1000, collapse to gene symbols, Mouse_Gene_Symbol_Remapping_MSigDB.v7.0.chip Chip platform, weighted enrichment statistic, Signal2Noise metric ranking for genes, real gene list sorting mode, and set size 10–1000.

T cell ATAC-seq

Mouse spleens were harvested from 3 WT and 3 KO mice, PBMCs were isolated using Ficoll separation, and naive CD4 T cells were isolated using Mouse Naive CD4+ T Cell isolation kit. Three vials of 200,000 cells each in 500uL cRPMI + 10% DMSO were prepared and shipped on dry ice to Genewiz to carry out ATAC-seq. The raw files were received and subsequently analyzed using Partek in which the following workflow was performed: base trimming, alignment via BWA, peak calling with MACS2, peak annotation, quantification, further annotation, differential analysis via GSA, and gene filtering based on expression value and q-value.

Mouse CD8 T cell perforin staining

For mouse CD8 T cell perforin staining experiments, splenocytes were harvested, followed by pan T cell isolation), and sorting out CD8s using an Aria cell sorter. The cells were then stimulated with 10 μg/mL plate-bound anti-CD3and 1.5 μg/mL anti-CD28 in a 96-well plate with 100,000 cells/well. After monitoring for 2–3 days, media supplemented with IL-2 (200 IU/mL) was used to split the cells and monitored via flow for perforin expression (PE) each day from this time point forward.

Human CD8 T cell CRISPR and perforin staining

PBMCs were isolated from healthy donor blood (buffy coat or single donors) by Ficoll separation, followed by Pan T cell magnetic isolation to isolate T cells. The T cells were then sorted on an Aria cell sorter to isolate CD8+ T cells specifically. The cells were then plated overnight and stimulated with 5 μg/mL plate-bound anti-CD3and 1 μg/mL anti-CD28 in suspension. After 24 hours the cells were harvested and 3–5 million were used for CRISPR. The gRNA and tracer were first combined and incubated at 37C for 30 minutes, followed by Cas9 and incubating at 37C for an additional 15 minutes. During this time the cells were spun down and resuspended in the appropriate amount of P3 Primary Cell Amaxa buffer and solution mixture. The gRNA/Cas9 mixture was then mixed with the cells and plated in the 4D-nucleofector plate. The cells were transfected using the setting EH-115 and 80uL of warm media (1:1 mixture of cRPMI : XVIVO + IL-2 (100IU/mL) was immediately added. The cells were incubated at 37C for 15 minutes before being transferred to 4mL of media in a T25 flask. Beginning at 24 hours later, the cells were monitored for viability and concentration each day, with more IL-2 supplemented media being added as needed. Cells were stained each day for L/D and perforin (PE) and flow cytometry was performed using either a Fortessa or MACSQuant machine.

Human mRNA Transfection

Human *ELF4* mRNA was generated from WT ELF4 and W250S ELF4 myc-tagged DNA plasmids with the HiScribe™ T7 ARCA mRNA Kit with tailing following the vendor-provided protocol. The mRNA was then further purified with the Monarch mRNA Cleanup Kit (50 μg) following the vendor-provided protocol. mRNA was stored at −80C until use for mRNA transfection. Human CD8 blasts were stimulated with 5 μg/mL plate-bound anti-CD3 and 1 μg/mL anti-CD28 in suspension following sorting from PBMCs. They were then maintained in culture with IL-2 supplemented media (100 IU/mL) for seven days before harvesting for transfection. mRNA transfections were performed using the Neon Transfection System (ThermoFisher). On the day of transfection, 1E6 cells were harvested per condition and washed twice with PBS. The cells were then resuspended in 9 μL of Buffer T and mixed with 1 μg of mRNA (2–3 μL depending on concentration of plasmid). The cells were then transfected with settings 2200V, 10ms, 2 pulses and immediately placed in 200 IU/mL IL-2 supplemented media (without antibiotics) and incubated at 37C. Expression of the myc tag and perforin was determined via intracellular staining and flow cytometry after 24 hours from the time of transfection.

PBMC and mouse BMDM macrophage experiments

Proteintech antibody used at 1:1000 for human ELF4 blots. For mouse bone marrow-derived macrophage (BMDM) experiments, bone marrow was harvested by centrifugation and plated in sterile petri dishes in complete DMEM media (DMEM with 55 μM beta mercaptoethanol, 10% FBS and 1% penicillin, streptomycin, and glutamine) supplemented with 20 ng/mL recombinant mouse M-CSF. Cells were cultured for one week, with fresh M-CSF supplied on day 4 and 6. On day 7, cells were harvested by trypsinization for 5 minutes at 37C, counted and plated at 1×10^6 cells per well of 6 well tissue culture plates in 3 ml of cDMEM supplemented with M-CSF overnight before stimulation. LPS was added at indicated concentrations. For Trem1 detection, cells were incubated for 60 minutes at 4C with anti-Trem1and subsequent flow cytometry analysis.

Patient PBMCs were isolated from fresh blood by passing over a ficoll gradient and collecting the leukocyte layer and plated at 0.4 million/ml in 96 well plates. LPS was added at 100 ng/mL concentration and supernatants were harvested 12 hours after stimulation. Culture supernatants were flash frozen in liquid nitrogen and thawed for analysis with BioLegend's Human Inflammation panel 1 according to the manufacturer's protocol. For intracellular flow cytometry of patient cells for IL-12p40, PBMCs were treated for 20 hours with 100 ng/mL LPS followed by 4-hour treatment with Monensin at 1:1000 dilution in non-tissue culture-treated 6-well plates. Cells were lifted by vigorous pipetting and gentle scraping with cell scrapers, washed twice in FACS buffer and fixed with fixation buffer for 20 minutes at room temperature in the dark. Cells were washed in 1x permeabilization wash buffer and stained overnight with anti-IL-12p40 PE. Cells were analyzed on a BD Fortessa.

CRISPR editing of human CD14+ monocyte-derived macrophages

PBMC were isolated as described before. CD14+ monocytes were sorted through CD14+ negative kit. CRISPR RNPs were prepared by annealing crisprRNA, tracrRNA, and Cas9 and transfected into cells with P3 Primary cell 4D-NucleofectorTMX kit. Cells were

cultured 7–9 days to differentiate to macrophages (1X IMDM, 20% Human AB Serum, Penicillin, Streptomycin, 1 mM Sodium Pyruvate). 2×10^5 /well were treated with 200 ng/mL LPS for 24h. Supernatants were assayed for IL-1β or CXCL1 by ELISA.

PRR-induced cytokine secretion

BMDMs were isolated KO, W250s or WT mice and cultured for seven days. 5×10^5 per well were treated with 20 ng/mL LPS, 10 μg/mL MDP), 50 μg/mL Poly(I:C), or 50 μg/mL β-glucan for 24 hr. Supernatants were assayed for IL-1β, IL-6, IL-12p70, IL-23 or CXCL1 ELISA.

Induction of LPS-induced sepsis

Endotoxic shock was induced in 6–8-week-old male Elf4 KO, W250S, and WT mice or 6–8-week-old heterozygous female Elf4 KO, W250S, and WT mice via i.p. injection of ultrapure LPS extracted from *Escherichia coli* at a dose of 2 mg/kg. In some experiments, 0.25 mg/kg recombinant mouse Trem-1 Fc fusion protein or control PBS was administered i.p. 1 h after LPS injection. Injected mice were monitored by Rodent thermometer TK-8851 (Braintree Scientific) at 0, 2, 4, 6 and 16 hours. Animals were scored at hourly intervals using the following criteria: score 0 = no symptoms; score 1 = piloerection, huddling; score 2 = piloerection, huddling, diarrhea; score 3 = lack of interest in surroundings, severe diarrhea; score 4 = decreased movement, listless appearance; and score 5 = loss of self-righting reflex. When mice reached a score of 5, they were humanely euthanized. Mouse blood was collected at 0, 4, and 24 hour timepoint for measurement of serum cytokines and chemokines. Eotaxin, TNF-α, IFN-γ, IL-1α, IL-1β, IL-6, IL-10, IL-12, IL-17, CCL3, CCL5, CXCL2, and CXCL10 were measured using the 32-Plex Mouse Cytokine/Chemokine Assay, IL-18, IL-23, IL-33, and IFN-β. Small intestine sections from mice were fixed with 10% neutral buffered formalin, embedded in paraffin, sectioned, and stained with hematoxylin and eosin (H&E).

ChIP-sequencing re-analysis

For ChIP-sequencing peak calls, ChIP Atlas (https://chip-atlas.org/) was used with previously published and analyzed data from Natoli et al.[13] and visualized using Integrated Genome Viewer (IGV_2.7.2) on the mm10 genome. Peak call was determined using a q value less than 0.01 for each of the genes highlighted in heat maps in Figure 5, for both untreated samples and for samples treated for 4 hours with LPS.

Statistical methods

Unpaired t-tests were used to determine significance for all ELISAs, *in vitro* luciferase assays, and RT-PCR analyses under the assumption that both populations have the same SD with two-tailed P values. Genes measured by RNA sequencing were filtered and ranked based on counts greater than 10, FDR values less than or equal to 0.1, and fold change greater than 1.5 shown in the volcano plots. Alternative filtering of the data is noted in figure legends. GSEA enrichment score (ES) values reflect the degree to which a gene is overrepresented at the top or bottom of a ranked list of genes where a positive ES indicates gene set enrichment at the top of the ranked list. The normalized enrichment score (NES)

normalizes ES for each gene set to account for the size of the set. The false discovery rate (FDR) is determined by comparing the tails of the observed and null distributions for the NES and all FDR q-values are less than 0.1. The mean expression value for each gene was calculated, followed by the use of the metric Signal2Noise to rank genes with respect to the two phenotypes. Signal2Noise uses the difference of means scaled by the standard deviation to analyze each categorical phenotype group of three samples or more. Pathway enrichment was determined by Ingenuity Pathway Analysis (IPA) utilizing p-values calculated by Fishers Exact Test and network bias correction. For pathway enrichment comparison, datasets were filtered by total counts greater than 10, FDR = 0.05 or 0.1 and fold change greater than 1.5 – 2 or less than −1.5 – −2.

Extended Data

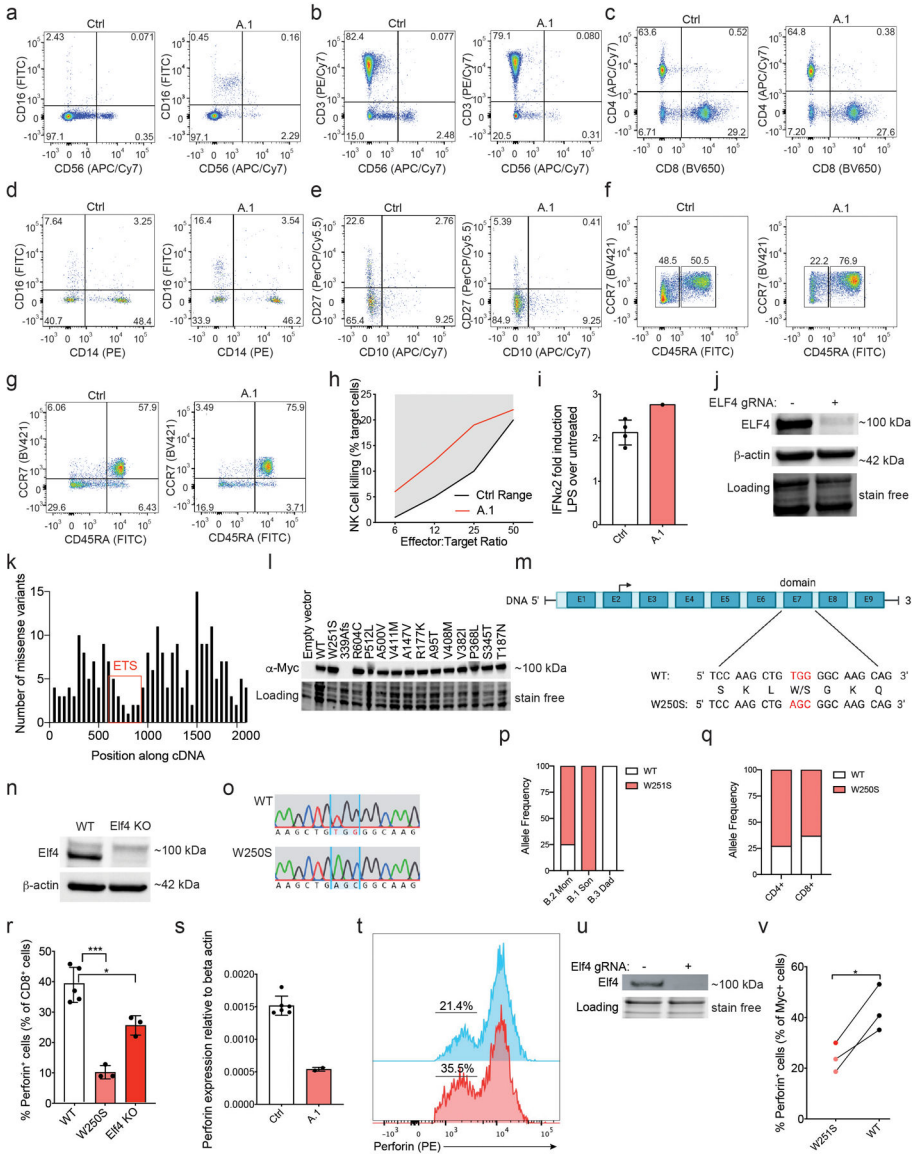

Extended Data Fig. 1. Extended DEX patient clinical and cellular findings and generation of *Elf4* KO and W250S mice.

(**a**) NK cell, (**b**) NKT cell, (**c**) $CD4^+$ and $CD8^+$ T cell, (**d**) monocyte, (**e**) B cell, (**f**) $CD4^+$ memory and naïve, and (**g**) $CD8^+$ memory and naïve flow cytometric immunophenotyping for the indicated markers on PBMCs from a healthy donor (Ctrl) and patient A.1. (**h**) NK cytotoxicity assay using PBMCs from patient A.1 (red) compared to the normal range (grey shading). (**i**) Human IFNα ELISA in supernatants of LPS-stimulated PBMCs from healthy donors (n=3) and patient A.1 (n=1). (**j**) Western blot on THP1 lysates for ELF4. (**k**) Histogram of missense variants in the gnomAD dabase in ELF4 gene. (**l**) Western blot on 293T cells overexpressing variants of ELF4 (myc-tagged) reported in gnomAD. (**m**) Schematic of mouse *Elf4*. (**n**) Western blot for Elf4 in mouse thymus. (**o**) Sanger sequencing genotyping of W250S mice. (**p**) Relative allele usage of B.2 (X/W251S) PBMCs. (**q**) Relative allele usage (X/W250S) of mouse $CD4^+$ or $CD8^+$ cells (**r**) Percentage of perforin+ $CD8^+$ T cells (WT n=6, W250S n=3, Elf4 KO n=3) 4 days with after anti-CD3 and anti-CD28. (**s**) Perforin gene expression in blasting $CD8^+$ T cells isolated from healthy controls and patient A.1 determined by qRT-PCR (Ctrl n=3, A.1 n=1). (**t**) Histogram displaying perforin expression in NT and ELF4 CRISPR-edited human CD8+ T cells after 10 days of IL-2. (u) Western blot showing CRISPR deletion of ELF4 from human CD8+ T cells by CRISPR. (v) Perforin expression determined by flow cytometry at 24-hour time point following overexpression of myc-tagged W251S and WT ELF4 mRNA in patient A.1, B.1 (pink), and C.1 (red) CD8+ T cells. Data are presented as mean +/− S.E.M. with two-tailed unpaired t-test (**r**) or paired t-test (**v**) *****p<0.05, **p<0.01, ***p<0.001, ****p<.0001, no marking indicates not significant.

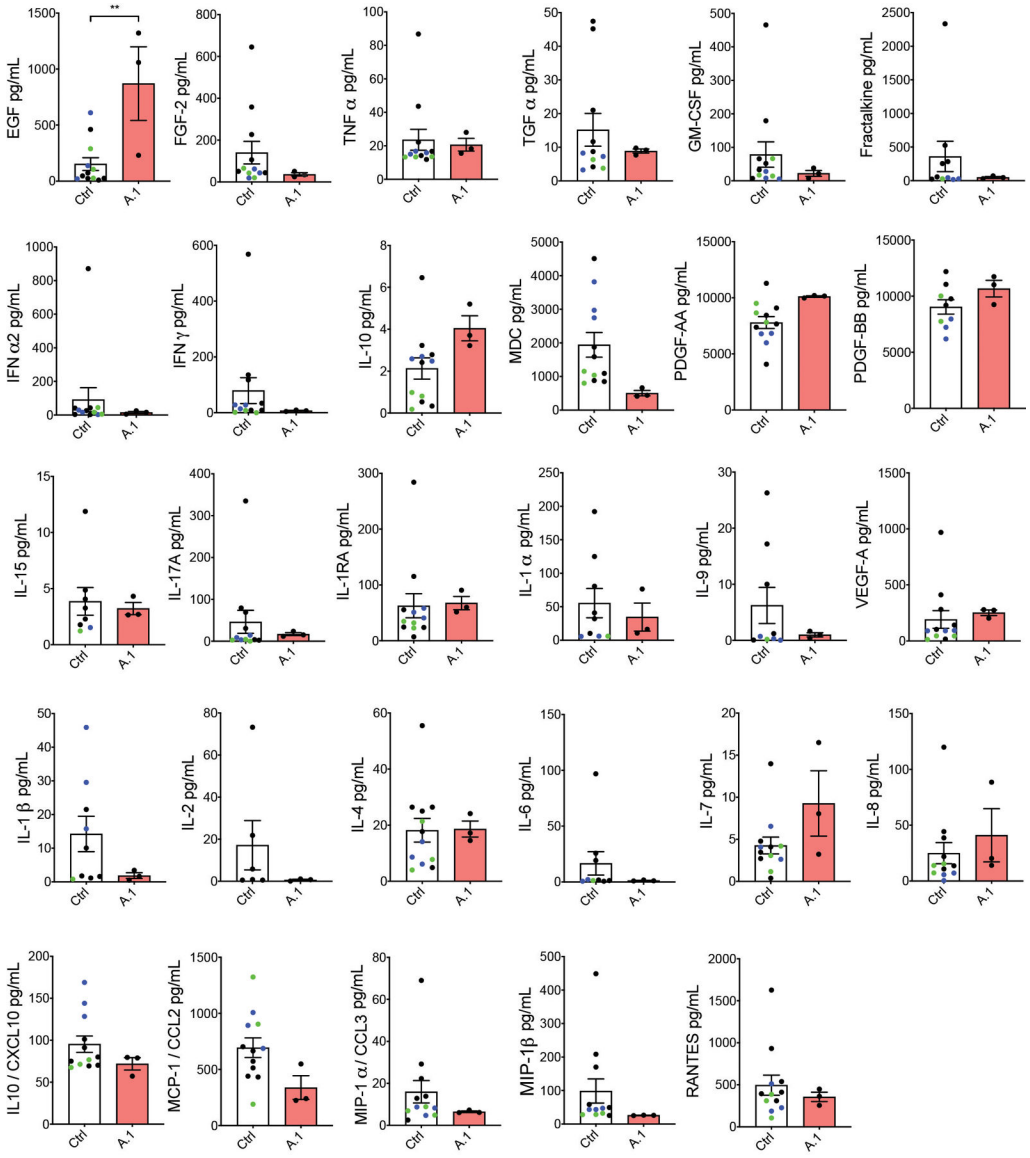

Extended Data Fig. 2. Extended serum analyses in patient A.1.

Concentrations of the indicated cytokine or chemokine in serum from independent blood draws of unrelated healthy controls (n = 4–6), patient A.1 (n = 3), mom (blue circles, n = 3), and dad (green circles, n = 1–3). Data from three independent experiments is presented as mean ± SEM. Statistical analysis was performed using two-tailed unpaired t-test. **p<0.01, no marking indicates not significant.

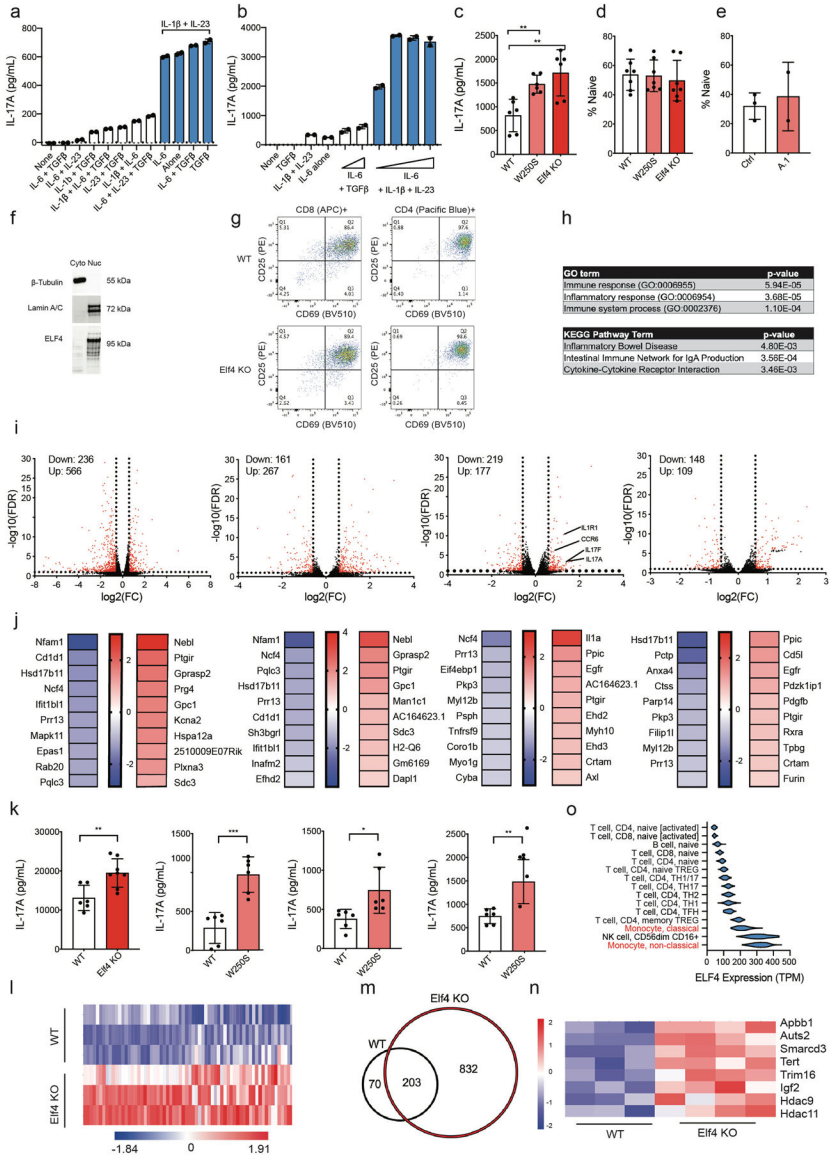

Extended Data Fig. 3. Extended data on T cell differentiation and gene expression.

ELISA for IL-17A from human CD4$^+$ cells (n=1). (**b**) ELISA for IL-17A from mouse CD4$^+$ T cells (n=1). (n=1). (**c**) Mouse IL-17A ELISA following naïve CD4$^+$ Th17 *in vitro* differentiation under non-pathogenic conditions (TGFβ + IL-6) WT n=3, W250S n=3, Elf4 KO n=3. (**d-e**) Percentage of mouse or human naïve CD4 T cells in spleen (WT n=3, W250S n=3, Elf4 KO n=3) or PBMC (Ctrl n=3, A.1 n=2), respectively. (**f**) Western blot of cytoplasmic (Cyto) and nuclear (Nuc) fractions of effector T cells. (**g**) Flow cytometry after treatment with anti-CD3 and anti-CD28 for 72 hours. (**h**) List of gene sets and pathways associated with the differentially expressed genes in Elf4 KO naïve CD4$^+$ T cells. (**i**) Volcano plots of differentially expressed genes in Elf4 KO (1) or W250S (2) versus WT mouse naïve CD4$^+$ T cells or W250S versus WT mouse *in vitro* differentiation Th17 cells after 48 hours under non-pathogenic (3) or pathogenic (4) conditions. (**j**) Top ten upregulated and downregulated genes in Elf4 KO or W250S CD4$^+$ T cells. Values shown as

log2(FC). (**k**) Naive CD4$^+$ T cells differentiated *in vitro* to Th17 cells. (**l**) Heat map showing Z-score summary of naive CD4$^+$ T cell ATAC-seq peak results filtered for genes with p-value < 0.01 and FC > 2. (**m**) Venn diagram displaying overlap between ATAC-seq peaks in Elf4KO and WT naive CD4$^+$ T cells. (**n**) Heatmap displaying genes involved in chromatin regulation that were differentially expressed by RNAseq (WT vs Elf4 KO) and also display differences in accessibility by ATACseq. (**o**) Reanalysis of DICE database [45]. ELISA data are from a minimum of three experiments, each dot representing one ELISA well with two wells/technical replicates per sample. A minimum of n=3 mice (biological replicates) was used for each genotype in mouse experiments. DEX patient samples represent blood from the same patient at different times. Data are presented as mean ± S.E.M. with two-tailed unpaired t-test *p<0.05, **p<0.01, ***p<0.001, ****p<.0001, no marking indicates not significant.

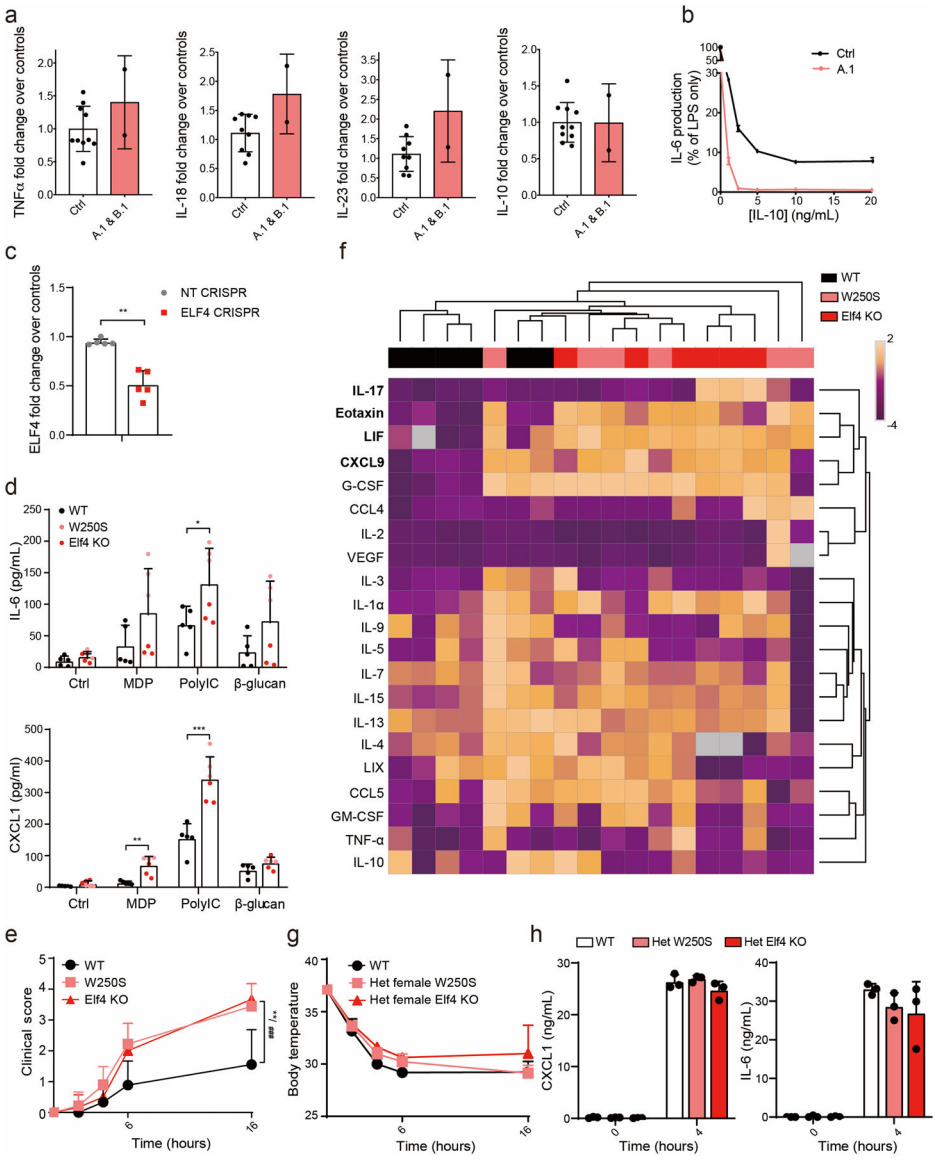

Extended Data Fig. 4. Extended data on monocyte/macrophage cellular responses.

Indicated cytokine measured in culture supernatants from LPS-stimulated human PBMCs. Data are combined from two independent experiments (patient A.1 vs 5 controls, and patient B.1 vs 5 controls) and expressed as fold change of patient values normalized to the average of the controls (n=13 healthy controls, n=2 A.1 independent experiments, n=1 B.1 experiment). (**b**) PBMCs from patient A.1 and a healthy donor control were treated with LPS alone or LPS and a titration of IL-10 for 12 hours, and IL-6 was measured in culture supernatants (n=1 patient and n=1 healthy donor control). (**c**) RT-PCR analysis of *ELF4* gene expression in monocyte-derived macrophages from healthy donors after CRISPR targeting (NT: non-targeting gRNA, ELF4: *ELF4* gRNA). (**d**) IL-6 and CXCL1 measured in culture supernatants from 24hrs MDP/PolyIC/β-glucan-stimulated BMDMs isolated from Elf4 KO, W250S, or WT mice. (**e**) Endotoxic shock was induced in groups of male WT and age-matched Elf4 KO and W250S mice by i.p. injection of 2 mg/kg ultra-pure (UP) LPS. Animals were scored for 0h, 2h, 4h, 6h and 16 h after LPS injection. (**f**) Concentrations of the indicated cytokine or chemokine in mouse serum 4 hr after i.p. LPS challenge. Analytes in red are significantly different between genotypes. (**g**) Endotoxic shock was induced in groups of female WT (n=3) and age-matched heterozygous females (Elf4 KO n=3 and W250S n=3) by i.p. injection of 2 mg/kg ultra-pure (UP) LPS. (**h**) Concentrations of the indicated cytokine or chemokine in mouse serum 4 hr after i.p. LPS challenge described in (G). Data are representative of three independent experiments and presented as mean ± SD. Statistical analysis was performed using two-tailed unpaired t-test. *p<0.05, **p<0.01, ***/###p<0.001, ****p<0.0001, no marking indicates not significant.

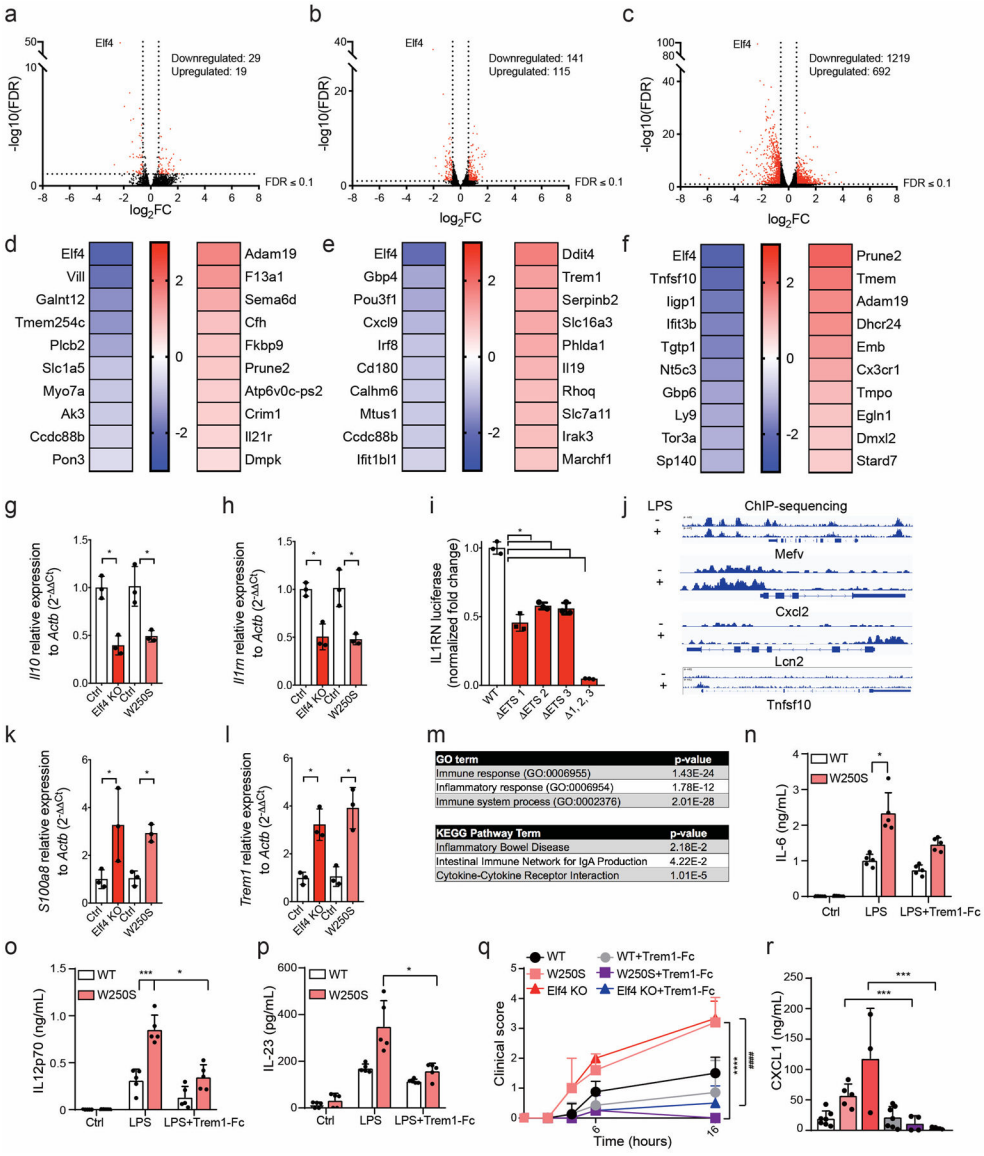

Extended Data Fig. 5. Extended data on macrophage gene expression and responses to Trem1 blockade.

(**a-c**) Volcano plots (-log10(FDR) vs fold change) of differentially expressed genes in Elf4 KO versus WT mouse BMDMs as indicated. (**d-f**) Heatmaps highlighting top 10 differentially expressed genes at each timepoint above. (**g-h**) RT-PCR for *Il10* and *Il1rn* in WT, Elf4 KO, or Elf4 W250S BMDMs at 16 hours after stimulation with LPS. For (g), (h), (k), and (l) n=3 wt and n=3 W250S mutant mice per group. (**i**) *IL1RN* reporter data as in Figure 5C but with three individual GGAA sites mutated to AAAA to assess the contribution of each to ELF4-driven transcriptional activation of *IL1RN* reporter, n=1 experimental replicate, representative of three independent experiments, ±SD. (**j**) ChIP-sequencing traces for Elf4 bound near the indicated gene in mouse BMDM without (−) and with (+) 4 hr LPS stimulation. (**k-l**) RT-PCR for *S100a8* and *Trem1* in WT, Elf4 KO, or Elf4 W250S BMDMs at 4 hours after stimulation with LPS. (**m**) Functionally enriched gene ontology and KEGG pathways of upregulated differentially expressed genes in Elf4

KO compared to WT BMDMs 16 hrs after LPS stimulation. (**n**-**p**) IL-6, IL-12p70, and IL-23 measured in culture supernatants at 24 hours after stimulation of indicated BMDMs with LPS or LPS and Trem1-Fc (n=5/group). (**q**) Endotoxic shock clinical score 16 hours after treatment (n=8,7 WT/WT+Trem1-Fc; n=3,4 Elf4 KO/Elf4 KO+Trem1 Fc; n=5,4 W250S/W250S+Trem1 Fc). (**r**) CXCL1 was measured in mouse serum at 4 hr after *in vivo* LPS challenge with the treatments indicated in (Q). Data are representative of three independent experiments and presented as mean ± SD. Statistical analysis was performed using two-tailed unpaired t-test. *p<0.05, **p<0.01, ***p<0.001, ****p<0.0001, no marking indicates not significant.

Supplementary Material

Refer to Web version on PubMed Central for supplementary material.

Acknowledgments:

The authors thank the patients and their families for participation in research and all clinical care staff for their contributions. We additionally thank P. Schwartzberg, P.-P. Axisa, and J.-M. Carpier for critical feedback. We acknowledge Prometheus for providing recombinant IL-2 used in T cell culture experiments and the Yale Cancer Center for support. We would like to thank Yale New Haven Hospital and Sara and Jeffery Buell for their support of the Pediatric Genomics Discovery Program. C.L.L. is funded by the Mathers Foundation, NIAID/NIH R01AI150913, Immune Deficiency Foundation, Hood Foundation, and Yale University. A.M.M. is funded by a Canada Research Chair (Tier 1) in Pediatric IBD, Canadian Institute of Health Research (CIHR) Foundation Grant, and NIDDK (RC2DK118640) grant and the Leona M. and Harry B. Helmsley Charitable Trust.

Data and materials availability:

RNA sequencing data were deposited in the Gene Expression Omnibus (GEO) database (GSE175569). Whole-exome sequencing data will not be made publicly available as they contain information that could compromise research participant privacy/consent. Information on the whole-exome sequencing raw data supporting the findings of this study is available from the corresponding author CLL upon request. Mice harboring the W250S or KO allele for *Elf4* are available from the corresponding author CLL upon request.

References

1. Bousfiha A et al. Human Inborn Errors of Immunity: 2019 Update of the IUIS Phenotypical Classification. J Clin Immunol 40, 66–81, doi:10.1007/s10875-020-00758-x (2020). [PubMed: 32048120]
2. Tangye SG et al. Human Inborn Errors of Immunity: 2019 Update on the Classification from the International Union of Immunological Societies Expert Committee. J Clin Immunol 40, 24–64, doi:10.1007/s10875-019-00737-x (2020). [PubMed: 31953710]
3. Adzhubei IA et al. A method and server for predicting damaging missense mutations. Nat Methods 7, 248–249, doi:10.1038/nmeth0410-248 (2010). [PubMed: 20354512]
4. Karczewski KJ et al. The mutational constraint spectrum quantified from variation in 141,456 humans. Nature 581, 434–443, doi:10.1038/s41586-020-2308-7 (2020). [PubMed: 32461654]
5. Rentzsch P, Witten D, Cooper GM, Shendure J & Kircher M CADD: predicting the deleteriousness of variants throughout the human genome. Nucleic acids research 47, D886–D894, doi:10.1093/nar/gky1016 (2019). [PubMed: 30371827]
6. Vaser R, Adusumalli S, Leng SN, Sikic M & Ng PC SIFT missense predictions for genomes. Nat Protoc 11, 1–9, doi:10.1038/nprot.2015.123 (2016). [PubMed: 26633127]

7. Poon GMK & Kim HM Signatures of DNA target selectivity by ETS transcription factors. Transcription 8, 193–203, doi:10.1080/21541264.2017.1302901 (2017). [PubMed: 28301293]
8. Sharrocks AD The ETS-domain transcription factor family. Nat Rev Mol Cell Biol 2, 827–837, doi:10.1038/35099076 (2001). [PubMed: 11715049]
9. Miyazaki Y, Sun X, Uchida H, Zhang J & Nimer S MEF, a novel transcription factor with an Elf-1 like DNA binding domain but distinct transcriptional activating properties. Oncogene 13, 1721–1729 (1996). [PubMed: 8895518]
10. Lacorazza HD et al. The ETS protein MEF plays a critical role in perforin gene expression and the development of natural killer and NK-T cells. Immunity 17, 437–449 (2002). [PubMed: 12387738]
11. Yamada T, Park CS, Mamonkin M & Lacorazza HD Transcription factor ELF4 controls the proliferation and homing of CD8+ T cells via the Kruppel-like factors KLF4 and KLF2. Nature immunology 10, 618–626, doi:10.1038/ni.1730 (2009). [PubMed: 19412182]
12. You F et al. ELF4 is critical for induction of type I interferon and the host antiviral response. Nature immunology 14, 1237–1246, doi:10.1038/ni.2756 (2013). [PubMed: 24185615]
13. Curina A et al. High constitutive activity of a broad panel of housekeeping and tissue-specific cis-regulatory elements depends on a subset of ETS proteins. Genes Dev 31, 399–412, doi:10.1101/gad.293134.116 (2017). [PubMed: 28275002]
14. Lee PH et al. The transcription factor E74-like factor 4 suppresses differentiation of proliferating CD4+ T cells to the Th17 lineage. Journal of immunology (Baltimore, Md. : 1950) 192, 178–188, doi:10.4049/jimmunol.1301372 (2014).
15. Bouchon A, Facchetti F, Weigand MA & Colonna M TREM-1 amplifies inflammation and is a crucial mediator of septic shock. Nature 410, 1103–1107, doi:10.1038/35074114 (2001). [PubMed: 11323674]
16. Uhlig HH et al. The diagnostic approach to monogenic very early onset inflammatory bowel disease. Gastroenterology 147, 990–1007.e1003, doi:10.1053/j.gastro.2014.07.023 (2014). [PubMed: 25058236]
17. Sobreira N, Schiettecatte F, Valle D & Hamosh A GeneMatcher: a matching tool for connecting investigators with an interest in the same gene. Human mutation 36, 928–930, doi:10.1002/humu.22844 (2015). [PubMed: 26220891]
18. Karczewski KJ et al. Variation across 141,456 human exomes and genomes reveals the spectrum of loss-of-function intolerance across human protein-coding genes. bioRxiv, 531210, doi:10.1101/531210 (2019).
19. Kircher M et al. A general framework for estimating the relative pathogenicity of human genetic variants. Nat Genet 46, 310–315, doi:10.1038/ng.2892 (2014). [PubMed: 24487276]
20. Flannigan KL et al. IL-17A-mediated neutrophil recruitment limits expansion of segmented filamentous bacteria. Mucosal immunology 10, 673–684, doi:10.1038/mi.2016.80 (2017). [PubMed: 27624780]
21. Revu S et al. IL-23 and IL-1beta Drive Human Th17 Cell Differentiation and Metabolic Reprogramming in Absence of CD28 Costimulation. Cell Rep 22, 2642–2653, doi:10.1016/j.celrep.2018.02.044 (2018). [PubMed: 29514093]
22. Stark MA et al. Phagocytosis of apoptotic neutrophils regulates granulopoiesis via IL-23 and IL-17. Immunity 22, 285–294, doi:10.1016/j.immuni.2005.01.011 (2005). [PubMed: 15780986]
23. Weaver CT, Elson CO, Fouser LA & Kolls JK The Th17 Pathway and Inflammatory Diseases of the Intestines, Lungs, and Skin. Annual Review of Pathology: Mechanisms of Disease 8, 477–512, doi:10.1146/annurev-pathol-011110-130318 (2013).
24. Okayasu I et al. A novel method in the induction of reliable experimental acute and chronic ulcerative colitis in mice. Gastroenterology 98, 694–702, doi:10.1016/0016-5085(90)90290-h (1990). [PubMed: 1688816]
25. Wirtz S, Neufert C, Weigmann B & Neurath MF Chemically induced mouse models of intestinal inflammation. Nat Protoc 2, 541–546, doi:10.1038/nprot.2007.41 (2007). [PubMed: 17406617]
26. Esplugues E et al. Control of TH17 cells occurs in the small intestine. Nature 475, 514–518, doi:10.1038/nature10228 (2011). [PubMed: 21765430]

27. Mandal P et al. Caspase-8 Collaborates with Caspase-11 to Drive Tissue Damage and Execution of Endotoxic Shock. Immunity 49, 42–55 e46, doi:10.1016/j.immuni.2018.06.011 (2018). [PubMed: 30021146]
28. Manthiram K, Zhou Q, Aksentijevich I & Kastner DL The monogenic autoinflammatory diseases define new pathways in human innate immunity and inflammation. Nature immunology 18, 832–842, doi:10.1038/ni.3777 (2017). [PubMed: 28722725]
29. Beura LK et al. Normalizing the environment recapitulates adult human immune traits in laboratory mice. Nature 532, 512–516, doi:10.1038/nature17655 (2016). [PubMed: 27096360]
30. Takeda AJ et al. Human PI3Kgamma deficiency and its microbiota-dependent mouse model reveal immunodeficiency and tissue immunopathology. Nature communications 10, 4364, doi:10.1038/s41467-019-12311-5 (2019).
31. Lu Z et al. MEF up-regulates human beta-defensin 2 expression in epithelial cells. FEBS letters 561, 117–121, doi:10.1016/s0014-5793(04)00138-3 (2004). [PubMed: 15013761]
32. Cao L et al. HIPK2 is necessary for type I interferon-mediated antiviral immunity. Sci Signal 12, doi:10.1126/scisignal.aau4604 (2019).
33. Seifert LL et al. The ETS transcription factor ELF1 regulates a broadly antiviral program distinct from the type I interferon response. PLoS pathogens 15, e1007634, doi:10.1371/journal.ppat.1007634 (2019). [PubMed: 31682641]
34. Guo B, Chang EY & Cheng G The type I IFN induction pathway constrains Th17-mediated autoimmune inflammation in mice. J Clin Invest 118, 1680–1690, doi:10.1172/JCI33342 (2008). [PubMed: 18382764]
35. Guarda G et al. Type I interferon inhibits interleukin-1 production and inflammasome activation. Immunity 34, 213–223, doi:10.1016/j.immuni.2011.02.006 (2011). [PubMed: 21349431]
36. Reboldi A et al. Inflammation. 25-Hydroxycholesterol suppresses interleukin-1-driven inflammation downstream of type I interferon. Science (New York, N.Y.) 345, 679–684, doi:10.1126/science.1254790 (2014).
37. Aksentijevich I et al. An autoinflammatory disease with deficiency of the interleukin-1-receptor antagonist. N Engl J Med 360, 2426–2437, doi:10.1056/NEJMoa0807865 (2009). [PubMed: 19494218]
38. Reddy S et al. An autoinflammatory disease due to homozygous deletion of the IL1RN locus. N Engl J Med 360, 2438–2444, doi:10.1056/NEJMoa0809568 (2009). [PubMed: 19494219]
39. Schenk M, Bouchon A, Seibold F & Mueller C TREM-1--expressing intestinal macrophages crucially amplify chronic inflammation in experimental colitis and inflammatory bowel diseases. J Clin Invest 117, 3097–3106, doi:10.1172/JCI30602 (2007). [PubMed: 17853946]
40. Garvie CW, Hagman J & Wolberger C Structural studies of Ets-1/Pax5 complex formation on DNA. Mol Cell 8, 1267–1276, doi:10.1016/s1097-2765(01)00410-5 (2001). [PubMed: 11779502]
41. McKenna A et al. The Genome Analysis Toolkit: a MapReduce framework for analyzing next-generation DNA sequencing data. Genome research 20, 1297–1303, doi:10.1101/gr.107524.110 (2010). [PubMed: 20644199]
42. Wang K, Li M & Hakonarson H ANNOVAR: functional annotation of genetic variants from high-throughput sequencing data. Nucleic acids research 38, e164, doi:10.1093/nar/gkq603 (2010). [PubMed: 20601685]
43. Crowley E et al. Prevalence and Clinical Features of Inflammatory Bowel Diseases Associated With Monogenic Variants, Identified by Whole-Exome Sequencing in 1000 Children at a Single Center. Gastroenterology 158, 2208–2220, doi:10.1053/j.gastro.2020.02.023 (2020). [PubMed: 32084423]
44. Pan J, Thoeni C, Muise A, Yeger H & Cutz E Multilabel immunofluorescence and antigen reprobing on formalin-fixed paraffin-embedded sections: novel applications for precision pathology diagnosis. Mod Pathol 29, 557–569, doi:10.1038/modpathol.2016.52 (2016). [PubMed: 26939874]

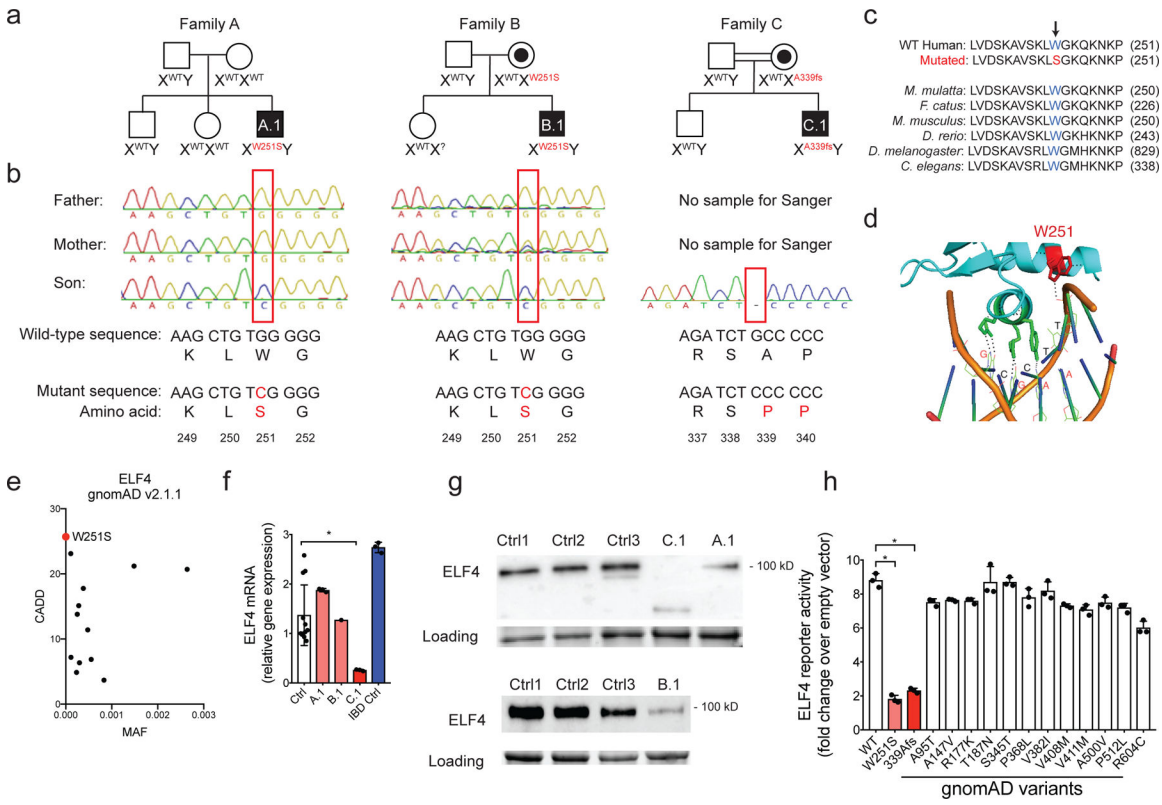

Figure 1. Loss-of-function variants in ELF4 identified in males with X-linked autoinflammatory disease.

(**a**) Three families with *ELF4* gene variants in affected males. wt: wild-type/reference; red W251S or A339fs variants; X: X chromosome; Y: Y chromosome. (**b**) Sanger sequence reads demonstrating locations of the variants. (**c**) Amino acid sequence alignment of ETS domains across species. Arrow indicates position of W251S variant. (**d**) Structure of ETS domain in complex with DNA (PDB 1K79 [40]) highlighting positioning of the residue analogous to human ELF4 W251S. (**e**) CADD scores versus minor allele frequency for the novel W251S patient-derived *ELF4* variant compared to *ELF4* variants present in males with MAF cutoff of $>10^{-4}$ from the gnomAD database. **f**) qRT-PCR analysis of ELF4 mRNA relative to GAPDH in PBMC samples from indicated subjects (n=3 patients with ELF4 variants and n=12 healthy donor controls) ±SD. Pink indicates W250S ELF4 variant, while red indicates frameshift/knockout. (**g**) Immunoblot for ELF4 in expanded T cell blasts from indicated subjects. 'Loading' indicates band from stain-free total protein imaging. (**h**) Activity of ELF4 variants (protein change indicated) from (**e**) and patient-derived variants ectopically overexpressed in 293T cells co-transfected with a transcriptional luciferase reporter as in, data are shown as one representative of three independent experiments, ±SD. [12]. Statistical analyses were performed using two-tailed unpaired T-test. *p<0.05, **p<0.01, ***p<0.001, ****p<0.0001, no marking indicates not significant.

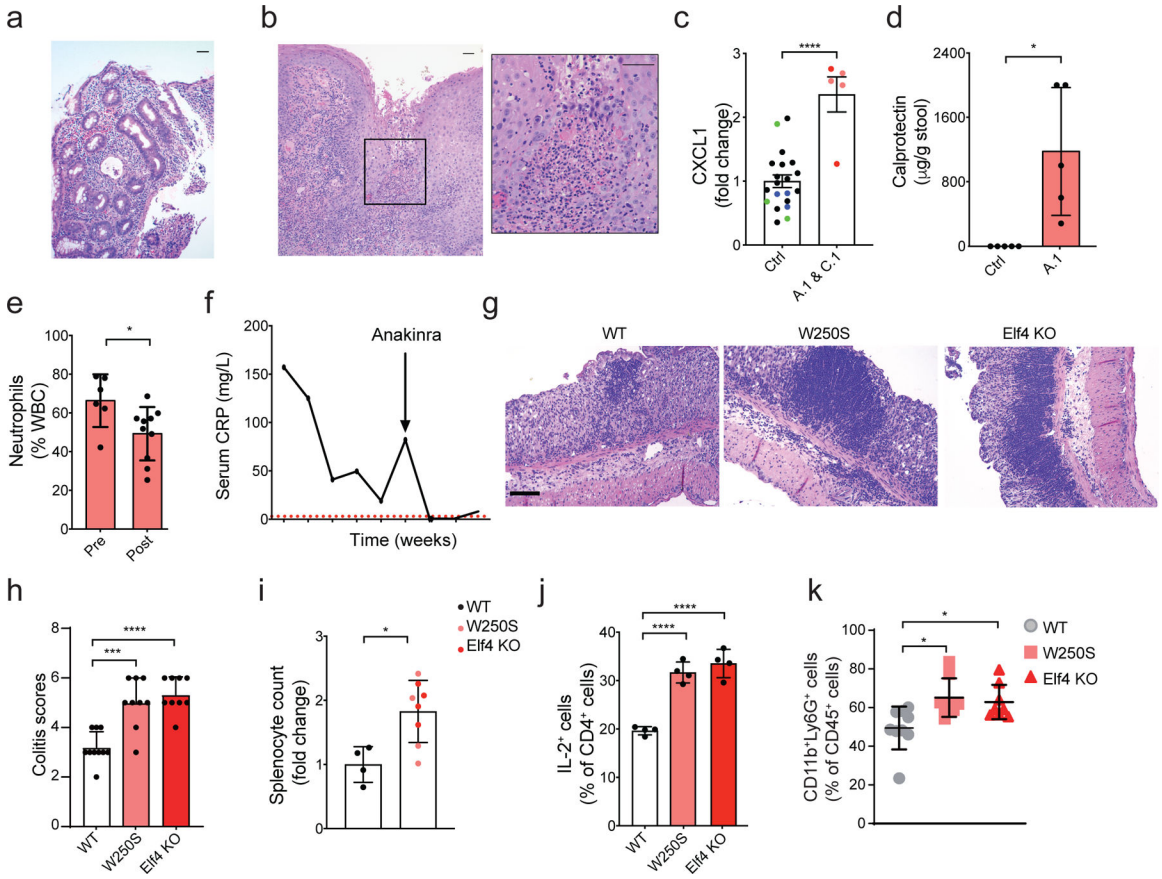

Figure 2. Inflammation *in vivo* and clinical response to anakinra.

(**a**) H&E micrograph of right colon of patient A.1 showing active colitis with crypt abscesses and ulceration. Scale bar: 50 μm. (**b**) H&E micrograph of cheek ulcer in patient B.1. Scale bar: 50 μm. (**c**) CXCL1 fold change in serum from independent blood draws of patient A.1 (n = 3), patient C.1 (n=2), unrelated healthy controls (n = 6), A.1 mom (blue circles, n = 3), and A.1 dad (green circles, n = 3). Data from three independent experiments is presented as mean ± SEM. Statistical analysis used two-tailed unpaired T-test. (**d**) Calprotectin (S100A8/S100A9 complex) measured in stool by ELISA from five independent samples of patient A.1 compared to five healthy donor controls ±SD. (**e**) Percentage of neutrophils from total white blood cells in patient A.1 pre- and post-anakinra (n=1 patient before and after treatment). (**f**) Serum CRP levels in patient A.1 shown over time. Red dotted line represents upper limit of normal levels. Data from three independent experiments is presented as mean ± SD. (**g-k**) Colitis was induced in groups of male WT (n=18) and age-matched Elf4 KO (n=13) and W250S (n=13) mice with 2% DSS for 7 days and harvested. (**g**) H&E micrograph of mouse colon. Scale bar: 50 μm. (**h**) Histological damage score from H&E images. (**i**) Splenocyte count. (**j**) Percentage of $CD4^+$ IL-2-producing splenic T cells. (**k**) Percentage of $CD11b^+Ly6G^+$ myeloid cells among $CD45^+$ cells in the colon. Data from three independent experiments is presented as mean ± SD with two-tailed unpaired T-test. *p<0.05, **p<0.01, ***p<0.001, ****p<0.0001, no marking indicates not significant.

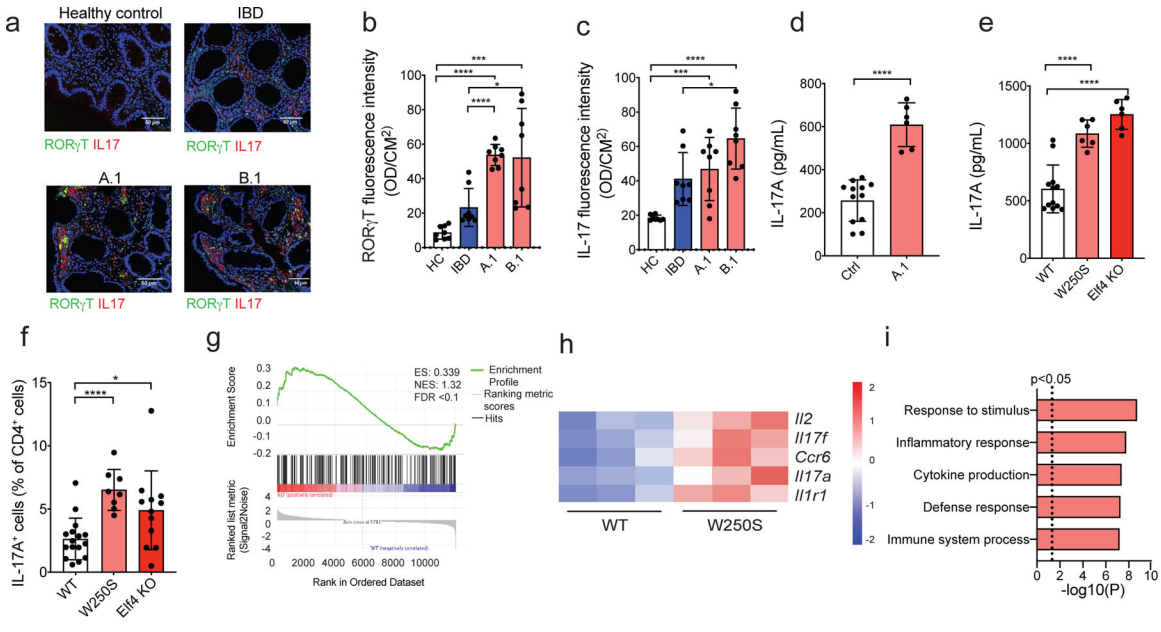

Figure 3. ELF4 deficiency augments T_H17 cell responses *in situ*, *in vitro*, and *in vivo*.

(**a**) Immunofluorescence staining of RORγT (green) and IL-17 (red) in healthy control, IBD, and patient A.1 and B.1 colons. (**b**) RORγT and (**c**) IL-17quantifications of staining in healthy control (white), IBD (blue), and patients A.1 and B.1 (pink). (**d**) Human IL-17A ELISA on patient A.1 (n=3) and healthy controls (n=6) after naïve CD4 T_H17 *in vitro* differentiation (IL-1 β and IL-23) for 7 days (**e**) Mouse IL-17A ELISA on naïve CD4 cells from WT (n=6), W250S (n=3), and Elf4 KO (n=3) littermates cultured under *in vitro* T_H17 conditions (IL-1β, IL-23, and IL-6) for 4 days. (**f**) IL-17A+ frequency of splenic CD4+ T cells from WT (n = 16), KO (n=12), and W250S mice (n=8) after 5 days of anti-CD3. (**g**) Gene set enrichment analysis of Elf4-deficient naïve mouse CD4 T cells for enrichment in 'regulation of inflammatory response' (GO:0050727). Each black line represents 1 gene (387 total, from GSE175569). (**h**) Heatmap of key DEGs in WT vs. W250S mice T_H17 cells differentiated *in vitro* ranked by p-value with most significant at bottom. Red and blue indicate extent of upregulation and downregulation, respectively (from GSE175569). (**i**) Gene ontology enrichment in genes upregulated by Elf4 at 48 hr of T_H17 *in vitro* differentiation (from GSE175569). ELISA data are from a minimum of three experiments, each dot representing one ELISA well with two wells/technical replicates per sample. A minimum of n=3 mice (biological replicates) was used for each genotype in mouse experiments. DEX patient samples represent blood from the same patient at different times. Data are presented as mean +/− S.E.M. with two-tailed unpaired t-test *p<0.05, **p<0.01, ***p<0.001, ****p<.0001, no marking indicates not significant.

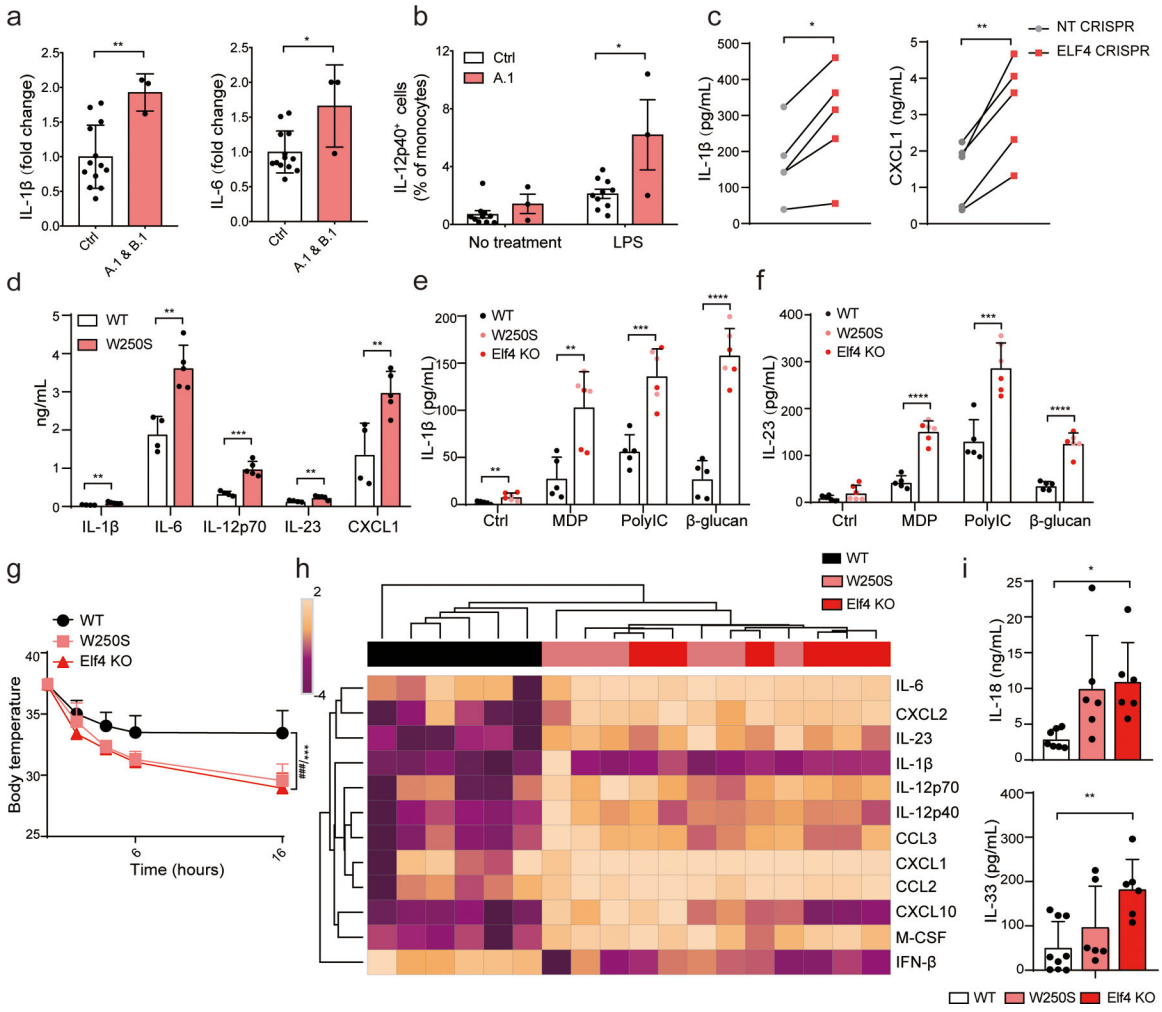

Figure 4. Innate inflammatory responses to PRR stimulation are augmented *in vitro* and *in vivo*.

(**a**) IL-1β and IL-6 measured in culture supernatants from LPS-stimulated PBMCs. Data are combined from two independent experiments (two patient A.1 blood draws vs 3–5 controls, and patient B.1 vs 5 controls) and expressed as fold change of patient values normalized to the average of the controls (n=13 healthy donor controls and n=3 patients). (**b**) Intracellular IL-12p40 staining by flow cytometry in gated monocytes after LPS stimulation of PBMCs for 24 hrs (including 6 hr with monensin), data shown for patient A.1 with three independent blod draws (n=3) compared to n=10 healthy donor controls. (**c**) IL-1β and CXCL1 measured in culture supernatants from 24hrs LPS-stimulated human macrophages; NT: non-targeting gRNA, ELF4: *ELF4* gRNA). Two-tailed paired t-test. (**d**) IL-1β, IL-6, IL12p70, IL-23 and CXCL1 measured in culture supernatants from 24hrs LPS-stimulated BMDMs isolated from W250S and WT mice. (**e-f**) IL-1β and IL-23 measured in culture supernatants from 24hrs MDP/PolyIC/β-glucan-stimulated BMDMs isolated from Elf4 KO and WT mice. (**g**) Endotoxic shock was induced in groups of male WT (n=9) and age-matched Elf4 KO (n=6) and W250S (n=9) mice by i.p. injection of 2 mg/kg ultra-pure LPS. Body temperature was monitored for 16 h after LPS injection. Data are representative of two independent experiments. (**h**) Differential abundance of the indicated cytokine in

serum from LPS-treated mice at 4 hr after challenge, depicting Z-scores. (**i**) Concentrations of the indicated cytokine in serum from LPS-treated mice at 24 hr timepoint. Data from three independent experiments is presented as mean ± SD with two-tailed unpaired t-test, *p<0.05, **p<0.01, ***/###p<0.001, ****p<.0001, no marking indicates not significant.

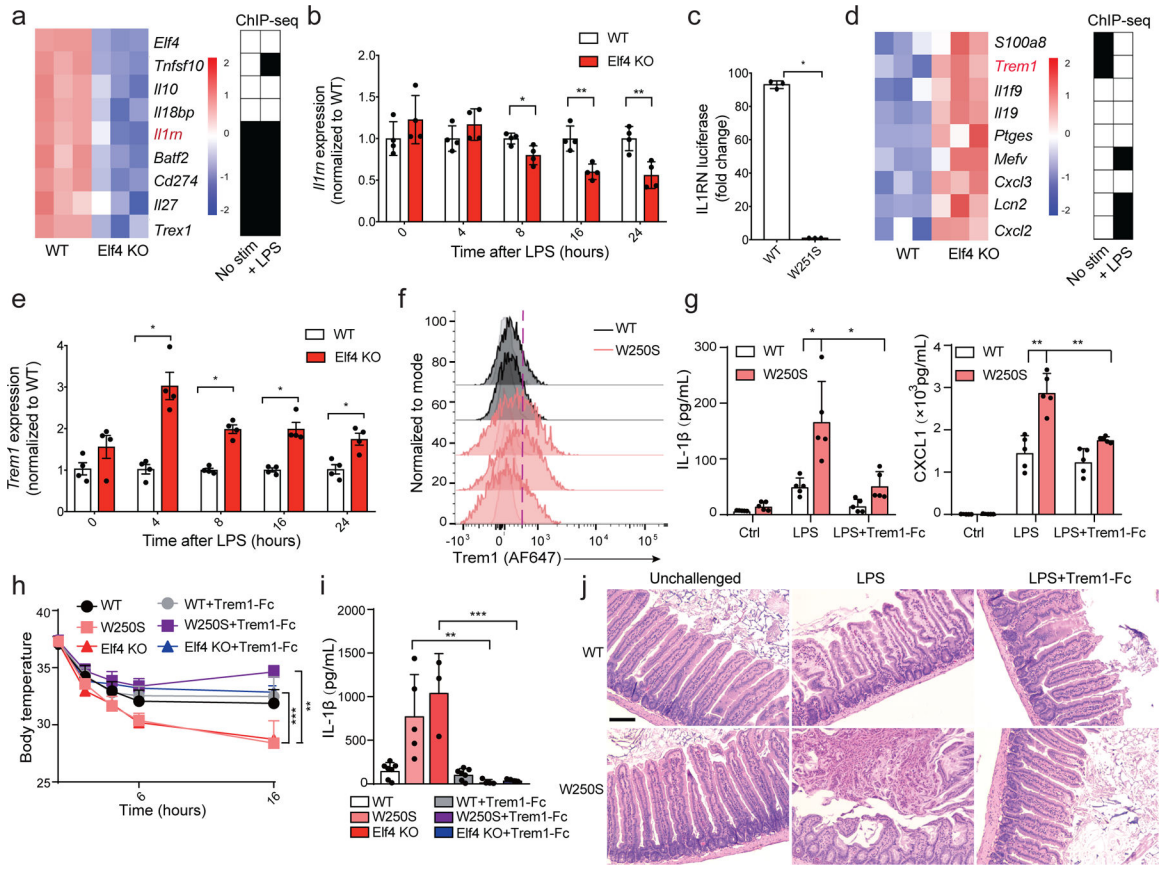

Figure 5. Elf4 in macrophages regulates anti- and pro-inflammatory genes including Trem1.

(**a**) Heatmap of genes low in Elf4 KO BMDMs 16 hours after LPS. Reanalysis of ChIP sequencing data from [13], baseline or 4 hours after LPS. (**b**) RT-PCR for *Il1rn* in mouse BMDMs after LPS with data normalized to average values of WT at each time point using ΔΔCt method, n=4 independent mice per group. (**c**) Human ELF4 acts on cis-regulatory sequences upstream of the secreted IL1RN transcription start site, as measured by luciferase reporter in 293 cells (data shown are one representative of three independent experiments ±SD).. (**d**) Heatmap of genes elevated in Elf4 KO BMDMs 4 hours after LPS (n=3 WT, n=3 Elf4 KO mice). Reanalysis of ChIP sequencing data as in (a). (**e**) RT-PCR for *Trem1* in mouse BMDMs after stimulation with LPS at time points given. Data are normalized as in (b). (**f**) Flow cytometric analysis of surface Trem1 on mouse BMDMs 24 hr after LPS stimulation *in vitro,* n=4 mice per group. (**g**) IL-1β and CXCL1 measured in culture supernatants from 24hrs LPS or LPS and Trem1-Fc-stimulated BMDMs isolated from W250S (n=5) and WT(n=5) mice. (**h**) Body temperature after endotoxic shock was induced in groups of male WT (n=8) and age-matched Elf4 KO (n=3) and W250S (n=5) mice by i.p. injection of 2 mg/kg LPS. Additional groups of mice (n=7 WT; n=4 Elf4 KO; n=4 W250S) received Trem1-Fc (0.25 mg/kg, i.p.) one hour after LPS injection. (**i**) IL-1β was measured in mouse serum at 4 hr timepoint. (**j**) Small intestine H&E stain for indicated genotypes and *in vivo* challenges. Scale bar: 50 μm. Data are presented as mean +/− SD with two-tailed

unpaired t-test, *p<0.05, **p<0.01, ***p<0.001, ****p<.0001, no marking indicates not significant.